Name Jonathan Tay Chien Ming

Degree: Masters of Engineering

Department: Department of Mechanical Engineering

Thesis title: Similarity of a Wall Jet with Uniform External Stream and Downstream Suction

Abstract

The two-dimensional turbulent wall jet in the presence of an external stream and downstream tangential suction at zero and adverse pressure gradients was experimentally studied. Streamwise velocity measurements show that the outer regions of the velocity profiles are practically self-similar with or without suction when the ratio of the maximum local and external stream velocities, $U_\infty/U_m \leq 0.8$. Self-similarity is lacking, however, in the inner region and is likely due to viscous friction at the wall hampering flow equilibrium. While the effect of downstream suction is negligible on the mean velocity profiles, the turbulent intensity profiles show that such suction reduces the turbulence level of the flow even far upstream of the suction slot when the streamwise pressure gradient is zero. With the adverse pressure gradient, this stabilizing effect of suction is inhibited. Both the imposed adverse pressure gradient and increasing jet Reynolds number result in a flow nearer equilibrium.

Keywords: Wall jet, tangential suction, tangential blowing, separation control, adverse pressure gradient, similarity.

SIMILARITY OF A WALL JET WITH UNIFORM EXTERNAL STREAM AND DOWNSTREAM SUCTION

JONATHAN TAY CHIEN MING

NATIONAL UNIVERSITY OF SINGAPORE

2008

SIMILARITY OF A WALL JET WITH UNIFORM EXTERNAL STREAM AND DOWNSTREAM SUCTION

JONATHAN TAY CHIEN MING

(B.Eng.(Hons.), NUS)

A THESIS SUBMITTED

FOR THE DEGREE OF MASTER OF ENGINEERING

DEPARTMENT OF MECHANICAL ENGINEERING

NATIONAL UNIVERSITY OF SINGAPORE

2008

Acknowledgements

The author would like to thank the following people who have helped so greatly in the completion of this project: the project supervisors, Prof. Khoo Boo Cheong and Dr. Tsai Her Mann for their patience and support through the various stages of this project, Dr. Hatsari Mitsudharmadi for his help and advice in the running of the experiments, as well as the staff of Temasek Laboratories for their generous aid whenever requested.

Table of Contents

Summary

Two-dimensional turbulent wall jets in the presence of an external stream and downstream tangential suction at zero and adverse pressure gradients were experimentally studied. Hot wire measurements of streamwise mean velocity distributions show that the outer regions of the velocity profiles are practically self similar for these jets with or without suction when the ratio of the maximum local and external stream velocities $U_\infty/U_m \leq 0.8$. Self-similarity is lacking however in the inner region, particularly very near the wall for both the mean and the turbulence intensity distributions and is likely due to viscous friction at the wall causing a lack of flow equilibrium. Increasing the jet Reynolds number reduces the effect of viscous friction, leading to an improvement in self-similarity, demonstrated by a significantly better collapse of the data.

While the effect of downstream suction is negligible on the mean velocity profiles, the turbulent intensity profiles show that such suction reduces the turbulence level of the flow even far upstream of the suction slot when the streamwise pressure gradient is zero.

Analytical studies have shown that for a wall jet with an external stream, in order to achieve self-similarity, the streamwise pressure gradient has to be adverse. Imposing an adverse pressure gradient close to that which is required indeed improves the self-similarity of the flow significantly, whether suction is present or not. However, the stabilizing effect of suction to reduce the turbulence intensities is inhibited with this imposed adverse pressure gradient. However, difficulty of the near

wall region to exhibit self-similarity of the mean and fluctuating velocity components is still encountered, though to a less significant extent.

Parameter scaling of the flow reveals the effect of Reynolds number on the flow development. Consistent trends are observed when the present study is compared to the work of Zhou and Wynanski (1993). Increasing Reynolds number increases the rate of jet growth as well as its rate of decay, likely due to increasing mixing and fluid entrainment.

List of Tables

List of Figures

List of Symbols

A_i = coefficient of *i*th correlation function

b = width of the jet slot

F_i = *i*th correlation function

J = excess kinematic momentum near the nozzle

$$\left(J = \int_0^\infty (U - U_\infty) U . dy = b(U_j - U_\infty) U_j - U_\infty^2 \theta_0 \right)$$

n_i = power coefficient of *i*th correlation function

R = dimensionless velocity parameter as defined by Eq. (3)

Re_j = jet Reynolds number ($Re_j = \frac{U_j . b}{\nu}$)

U = local mean velocity

U_j = jet velocity at the nozzle exit

U_m = local maximum velocity in the jet

U_∞ = freestream velocity

U_0 = (U_m - U_∞)

U_τ = friction velocity ($U_\tau = \sqrt{\tau_w / \rho}$)

u' = fluctuating velocity component in streamwise direction

u'_{rms} = root mean square of u'

x = streamwise distance measured from the nozzle

y = normal distance to the wall

y_m = normal distance of the position of maximum local velocity to the wall

y_0 = normal distance from the wall above the point of maximum velocity where the local velocity is reduced to one-half of its maximum value.

z = spanwise distance measured from center line of the test surface

θ_0 = momentum deficit at $x = 0$ ($\theta_0 = \left[\int_0^{\delta} \left\{ \frac{U}{U_\infty} \left(1 - \frac{U}{U_\infty} \right) \right\} dy \right]_{x=0}$)

ν = kinematic viscosity of the fluid

ξ = dimensionless distance from the nozzle ($\xi = \frac{xJ}{\nu^2}$)

ρ = density of the fluid

τ_w = shear stress at the wall

Chapter 1: Introduction

1.1. Background

There is considerable interest in the control of separated flow over airfoils at high angles of attack as this has significant impact on the performance of flight vehicles. While much of previous efforts have been based on passive methods of flow control such as through the use of vortex generators, recent interests have shifted to the use of active methods of flow control in the hope of minimizing the additional drag associated with conventional passive methods. The aim of these efforts is to control the flow so that it does not separate over an aerodynamic surface even at high angles of attack beyond the usual post-stall regime where a significant adverse pressure gradient is encountered. Flow attachment at such high angles of attack would allow significantly higher maximum lift coefficients to be attained.

Many previous attempts have been made to control the boundary layer flow through the use of blowing and suction to prevent separation (Wang and Sun 2000, Avi et al. 2004). Such methods of momentum transfer have often been done perpendicularly to the wall surface, either through a porous wall, or through slots or holes in the wall. Uniform blowing is found to decrease the skin friction over the blown area and increase the turbulence intensity while uniform suction increases skin friction with a reduction in turbulence intensity (Park and Choi 1999). Even small magnitudes of blowing and suction can significantly affect the skin friction and turbulence intensities above and downstream of the slot (Park and Choi 1999).

In some cases, blowing is done tangentially to the wall surface. This has been commonly applied to control the boundary layer over airfoils. Blowing is commonly applied either near the leading edge of the airfoil (Heap and Crowther 2003) or near the trailing edge (Englar 2000). By energizing the air near the surface of the airfoil boundary layer, flow separation can be delayed or even prevented in the presence of a significant adverse pressure gradient. This allows the airfoil to be operated at a higher angle of attack without stalling, or the lift coefficient of the airfoil may also be otherwise increased by deflecting the blown air downwards. In these cases of tangential blowing, the tangentially injected fluid essentially behaves as a wall jet.

The use of a wall jet for mixing the fluid from the jet with the ambient flow for the purpose of flow control is well known (Gad-el-Hak and Bushnell 1991). It is usually created by injecting fluid along a wall at a velocity higher than that of the ambient flow. The shear between the main free stream and the jet creates strong turbulence diffusion and mixing, thus providing the lateral transport of energy from the jet to the freestream for it to remain attached even at large angles of attack. The stall margin is hence significantly enhanced. The turbulent wall jet is an effective flow separation control technique but being an active control method, it requires direct energy expenditure.

A recent method that holds great promise in reducing the energy required is the co-flow jet (CFJ) airfoil proposed by Zha and his colleagues (Zha and Paxton 2006, Zha and Gao 2006, Zha et. al. 2006a, Zha et. al. 2006b). Figure 1.1 shows a schematic of this co-flow jet concept employed on an airfoil. It was proposed that a significant reduction in energy penalty can be achieved if the wall jet can be supplemented with

a suction port. The wall jet is injected tangentially on the upper surface of an airfoil near the leading edge and at the same time the same amount of mass flow is sucked from near the trailing edge. Compared with using just the wall jet alone which dumps away the mass flow, there can be efficiency gains for the overall airframe-propulsion system if the flow is recirculated.

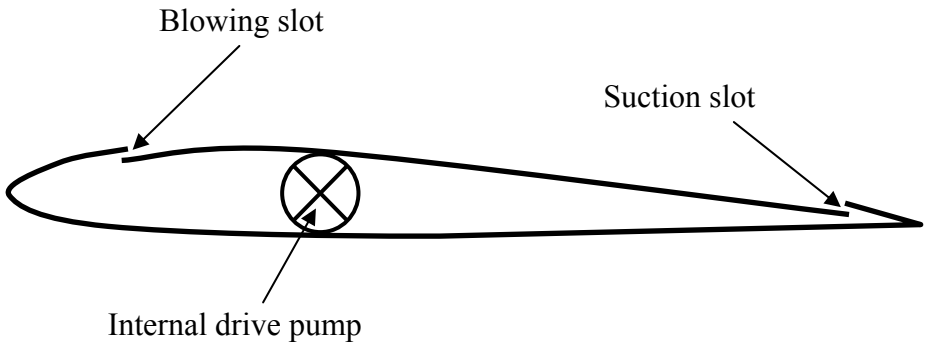

Figure 1.1. Airfoil employing co-flow jet.

Moreover it appears that the suction port also helps in flow attachment despite the severe adverse pressure gradient on the upper surface of the airfoil at high angles of attack. The overall lift on the airfoil is significantly enhanced as a result of the augmented circulation. This enhancement was shown to be over 3 times for the maximum lift coefficient attainable for a NACA 0025 airfoil (Zha and Gao 2006) when the CFJ concept was employed. A small amount of thrust is also generated by the action of the blowing and suction. However, this is not an effective way to generate thrust and the aim of achieving a high lift coefficient beyond the uncontrolled airfoil flow case remains the main attraction of the CFJ method.

While the concept of using both blowing and suction has been demonstrated (Zha and Paxton 2006), the details of the wall jet development in the presence of the external stream and tangential suction have not been examined in detail. For the wall jet with and without the presence of the external stream, there has long been the suspicion that there should be some kind of similarity solution for a plane wall jet. However, attempts to identify such a solution have not been totally successful. The presence of the no-slip condition precludes the possibility of similarity solutions for the entire flow (George et. al. 2000).

However, there still appears to be consensus that there are at least two regions within a wall jet, an inner region and an outer region (Townsend 1976). The inner region extends from the solid wall to the point above the wall where the velocity is maximum (y_m) and resembles a normal boundary layer flow. The outer region covers the part from the point of maximum velocity (y_m) to the outer edge of the jet and resembles a free-shear layer. The interaction of large-scale structures in the outer layer with smaller scales in the inner layer results in a complicated flow field and determines the development of the wall jet. Significantly the point at which the shear stress changes sign does not coincide with the position where the vertical velocity gradient is zero but lies slightly closer to the wall within the inner region (Launder and Rodi 1981).

Traditionally, the mean flow velocity distribution is scaled such that its rate of spread and the decay of the maximum velocity in the direction of streaming are dependent on the nozzle dimension whereas the velocity scale is the efflux velocity at the nozzle exit. Kruka and Eskinazi (1964) found that similarities exist in both the

inner and outer layers for mean as well as turbulent quantities. However, the same scales do not apply to both these layers. They showed that for the mean measurements, the flow was divided at the maximum velocity U_m location, while for the statistical quantities the flow was divided at the location where $\overline{uv} = 0$.

Narasimha *et al*. (1973) however suggested that the initial momentum flux and the viscosity of the fluid for the wall jet in quiescent surroundings should be used as length and velocity scales. Wygnanski *et al*. (1992) found that these scales are also useful for eliminating the Reynolds number Re_j dependence of the local scales and allow the estimation of τ_w from the momentum integral equation. Recently, George *et al*. (2000) revealed that both the inner and outer regions become asymptotically independent of Reynolds number and reduce to similarity solutions of the inner and outer boundary layer equations in the limit of infinite Reynolds number. This leads to the conclusion that there are no scaling laws that can perfectly collapse the data at finite Reynolds number. Barrenblatt *et al*. (2005) also confirmed that a single self-similar structure in the wall jet, to which a single scaling law can be applied, does not exist. Instead they suggested that the wall jet consists of two self-similar flow layers described by significantly different scaling laws and separated by a mixing layer where the velocity is close to the maximum.

In contrast with the situation of the wall jet in still air, plane wall jets in a uniformly moving external stream do not exhibit strict self-preserving behavior (Launder and Rodi 1981). Nevertheless for engineering purposes, Patel (1962) was able to suggest a scaling that allows a satisfactory collapse of mean velocity quantities. In his suggested scaling, the vertical coordinates were scaled by the

vertical distance from the wall to the location where the quantity of $(U-U_\infty)/U_0 = 0.5$, and the velocities were scaled by U_0. Figure 1.2 shows the physical meanings of these symbols commonly used in wall jet studies. This yielded a scaling which is valid over the entire range of the flows studied as well as for various ratios of external stream to jet exit velocity.

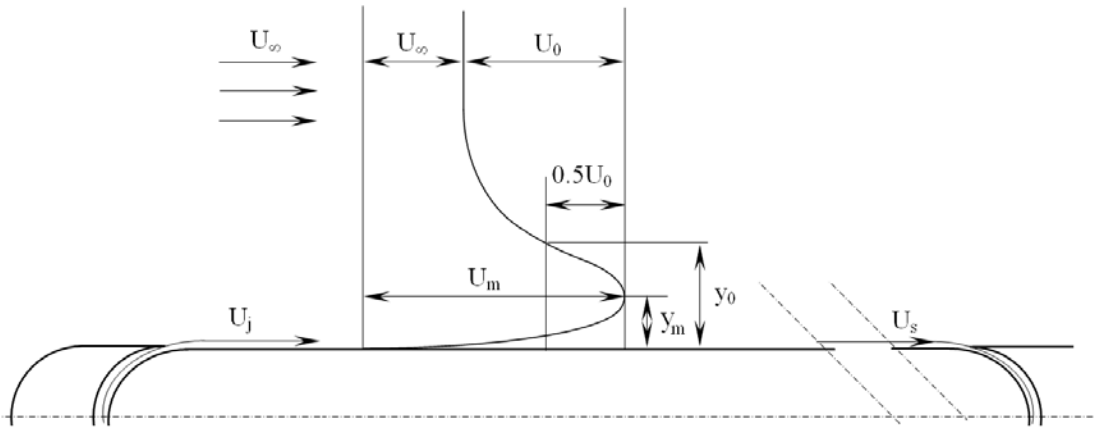

Figure 1.2. Common scaling parameters used with wall jets.

Zhou and Wygnanski (1993) similarly used U_0 to scale the mean velocities in the outer region, but another velocity scale U_m was used for the inner layer due to the no-slip condition at the wall resulting in positions where the local U might be less than U_∞. They found that this scaling allows the wall jet to appear self-similar in the presence of a uniform external stream provided the ratio of the external stream velocity to the local maximum velocity is less than 0.5 ($U_\infty/U_m < 0.5$).

1.2. Objective

Although the literature on the wall jet is extensive, none of the wall jet studies previously mentioned was conducted in the presence of both a uniform external

stream and tangential suction located downstream such as would be encountered in a co-flow jet. Thus the aim of the present study is to contribute further to the understanding of the development of the wall jet flow in the presence of an external stream and tangential suction as implemented in the CFJ concept.

Chapter 2: Experimental Setup

The experiments were carried out in a low speed blow down wind tunnel facility with a test section measuring 450mm by 450mm in cross-section. A flat plate spanning the entire width of the test section is positioned with its centerline 100mm above the tunnel floor. The flat plate is 100mm thick to enclose the necessary piping for the blowing and suction slots as well as the settling chambers required to ensure adequate mixing for 2-D flow at the slot exits. This means that a distance of 300mm remains between the plate upper surface and the wind tunnel roof when the plate is horizontal. A rounded leading edge with a constant radius of 50mm is used to mimic the blunt leading edge of a typical subsonic airfoil. Figure 2.1 shows the schematic layout of this test section as described.

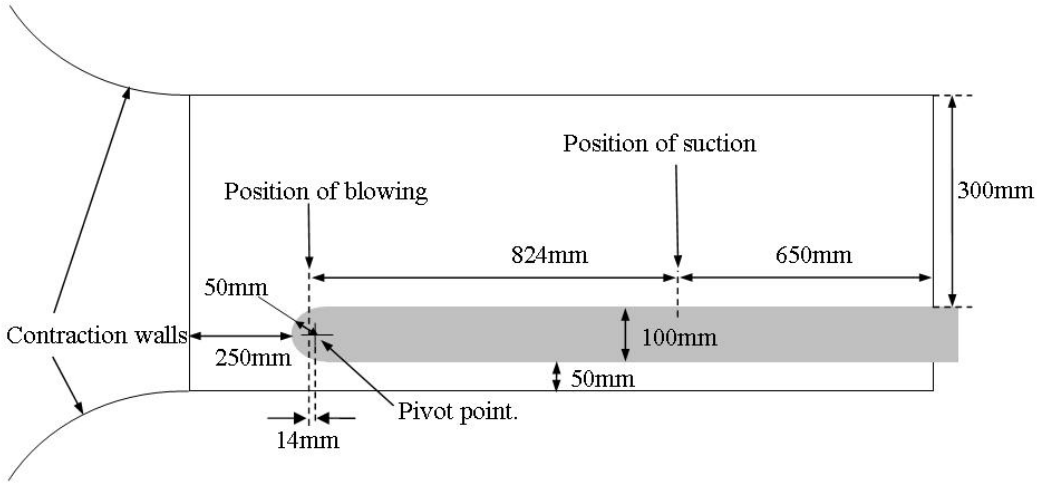

Figure 2.1. Schematic of test section.

A pivot was located at the center of curvature of the rounded leading edge to allow the plate to rotate and pivot the downstream portion of the plate downwards to create a diffuser type flow and create an adverse streamwise pressure gradient over the plate.

Measurements of the flow was done with the plate horizontal for zero pressure gradient flow and with it inclined at about 15^{o} for an adverse pressure gradient flow condition. This resulted in a pressure gradient sufficiently adverse to create separated flow over the top surface of the plate. This situation mimics what happens over the top of an airfoil at angles of attacks at or beyond stall, for which the CFJ concept of flow control was intended for.

For the cases with zero pressure gradient studied, the mean velocity of the external stream (U_{∞}) is constant at about 5.5m/s over the flat plate. For the cases with the adverse pressure gradient, the external stream is constant at about 5.5m/s at the position directly above the blowing slot.

The blowing slot is located about 14mm horizontally ahead of the center of curvature of the rounded leading edge as shown in Figure 2.2 and has a width *b* of 2mm and spans 425mm of the test section, 212.5mm each side of the centerline. A suction slot with width *s* of 5mm is situated 824mm, or 412b downstream of this blowing slot and also similarly spans 425mm of the test section width.

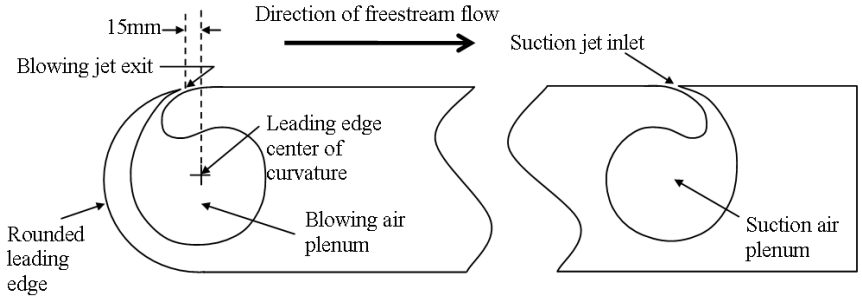

Figure 2.2. Blowing and suction slot details.

The flat plate surface extends for another 650mm beyond the suction slot to the end of the wind tunnel test section for the zero pressure gradient case and 700mm for the adverse pressure gradient case. The difference in lengths is due to the inclination of the test plate required to create an adverse pressure gradient as shown in Figure 2.3.

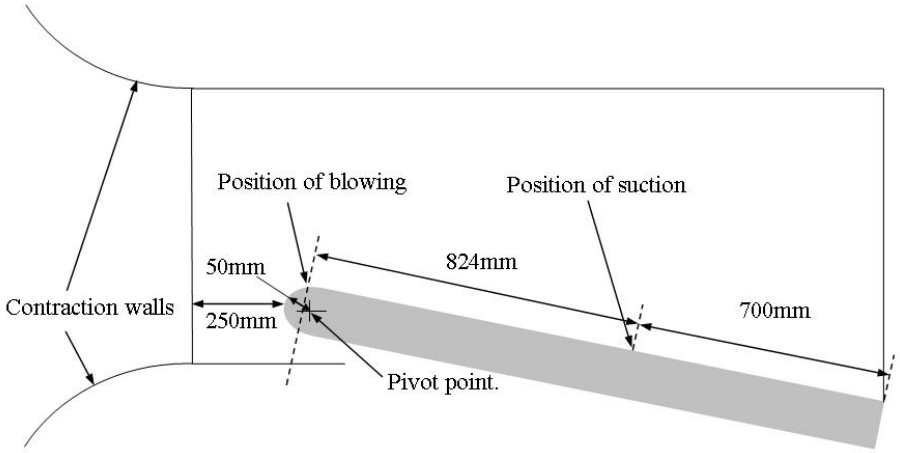

Figure 2.3. Configuration of test section with adverse pressure gradient imposed.

Air for the blowing slot was provided by a compressor, controlled and monitored via a pressure regulator and a floating element flow meter connected in series in between the compressor and the blowing slot. Suction power was provided by a throttle controlled vacuum pump and measured with a flow meter in series. Air was fed and removed from the test set-up from both sides of the air plenums shown in Figure 2.2. To ensure 2-D uniformity of the flow at the blowing and suction slots, the air plenums were filled with a coarse sponge to speed up the mixing of the flow within the air plenums.

Two jet exit velocities were used in this study and they were estimated to be about 13.5m/s and 21m/s from hot-wire measurements made near the blowing slot. The

suction flow velocity could not be determined using hot-wire anemometry due to the relatively larger suction slot resulting in a lower flow velocity as well as the fact that the suction slot acts similar to a sink source with the flow entering the suction slot from all directions in the plane perpendicular to the slot spanwise axis. This multi-directional suction flow results in even lower local flow velocities around the suction slot and thus resulted in the difficulty in ascertaining the flow velocity at the slot accurately. While inserting the hot-wire probe into the slot may yield some results, it was not attempted since inserting the relatively large probe into a relatively small suction slot will disturb the flow sufficiently to yield an inaccurate measurement of the suction flow velocity. Instead the volume flow rate applied was kept constant with that of the blowing rate for each set of experiments and the suction velocity estimated from the mean bulk velocity required to maintain the particular flow rate was 5.4m/s and 8.4m/s for the two jet velocities studied. The resulting jet Reynolds number Re_j based on the jet velocities at the blowing slot and its width b is about 1730 and 2660, respectively.

Hot wire measurements are made using a 55P15 hot-wire probe from Dantec Dynamics and operated in constant temperature mode with an overheat ratio of 1.8. Hot wire data was sampled by a Data Translation DT3010 data acquisition board at 6 kHz for 2^{16} data points for each time history giving a sampling time of 10.9 seconds.

This probe was regularly calibrated in situ against a pitot-static probe connected to an inclined manometer and placed next to it in the external stream. This pair of probes was positioned high above the leading edge of the flat plate to minimize any effects from the growing boundary layer on the plate below. The pitot-static tube used for

calibration was also at the same time connected to a Setra 239 pressure transducer for its simultaneous calibration. Since the inclined manometer used has a full-scale range of zero to 15mm H_2O, it was not sufficiently accurate for the measurement of low flow velocities using the pitot-static tube. However, because the positions where velocity measurements are to be carried out in the study include points very near the wall where the flow velocity is very low, the hot-wire probe would also require calibration for low flow velocities. Since the inclined manometer is not sufficiently accurate for this, the readings from the calibrated pressure transducer was used to calibrate the hot-wire probe at low velocity flows. The pressure transducer used has a full scale reading of 12.7mm H_2O and is sufficiently accurate at low flow velocities due to the linear relationship between its output signal and the applied pressure. A 4^{th} order polynomial curve was chosen to fit the obtained calibration points for the hot-wire probe as the commonly used King's law relationship and its variants are inaccurate at lower flow velocities when natural convection becomes significant, though not necessarily dominant. The sampling time of the hot-wire probe for calibration purposes was extended to 21.8 seconds to ensure an accurate calibration. The pitot-static tube used for calibration was subsequently removed after calibration of the hot-wire probe during the actual experimental runs.

A computer controlled traverse system with a resolution of 0.6×10^{-3}mm in both the y and z directions is used to move the hot-wire probe within the flow field. Velocity measurements were made at locations $22.5 < x/b < 430$ along the plate centerline downstream of the blowing slot, where x denotes the streamwise coordinate downstream from the blowing slot.

The side walls of the wind tunnel are largely made from transparent Perspex pieces except for some aluminum supports used to support the test plate above the wind tunnel floor. The transparent side walls allow optical access for flow visualization. Tuft flow visualization was carried out to observe the extent of the flow separation when the adverse pressure gradient was imposed by tilting the test plate. An aluminum rod with an airfoil cross-section was inserted through the roof of the wind tunnel into the test section and on it is glued an array of eight thin cotton threads spaced at 20mm intervals. A symmetrical airfoil cross-section was chosen for the rod to minimize any disturbance to the flow due to its presence. This rod was lowered from about 90mm above the test surface in discrete steps of 5mm down onto the test plate while a photograph of the resulting tuft patterns was taken at each step. A Nikon D100 camera was used to take these photographs. A slow shutter speed of about 1/8 second was used to obtain a representation of the mean tuft patterns over time. These photographs were subsequently superimposed upon each other to further obtain a more accurate representation of the mean flow field.

Table 2.1 below tabulates the test matrix for the present study for which the seven sets of velocity measurements are presented. Set No. 1 refers to the baseline case with no jet and suction applied on a flat test plate with zero streamwise pressure gradient over its surface.

Table 2.1 Test matrix

No.	Pressure Gradient	Re_j	Downstream Suction
1	Zero	-	No
2	Zero	1730	No
3	Zero	1730	Yes
4	Zero	2660	No
5	Zero	2660	Yes
6	Adverse	2660	No
7	Adverse	2660	Yes

Chapter 3: Results and Discussions

3.1. Zero pressure gradient case

3.1.1. Validation of zero pressure gradient and 2-D flow condition

Figure 3.1 shows the mean velocity profile at x/b = 341.5 over the test plate at test conditions with a zero stream wise pressure gradient in wall coordinates, commonly used in boundary layer studies. This position was arbitrarily chosen to be sufficiently far downstream of the leading edge for the boundary layer to develop. Also shown for comparison is the result from Bruns *et al.* (1992). The very good agreement between both sets of data gives further confidence in the accuracy of the measurements presented in this study.

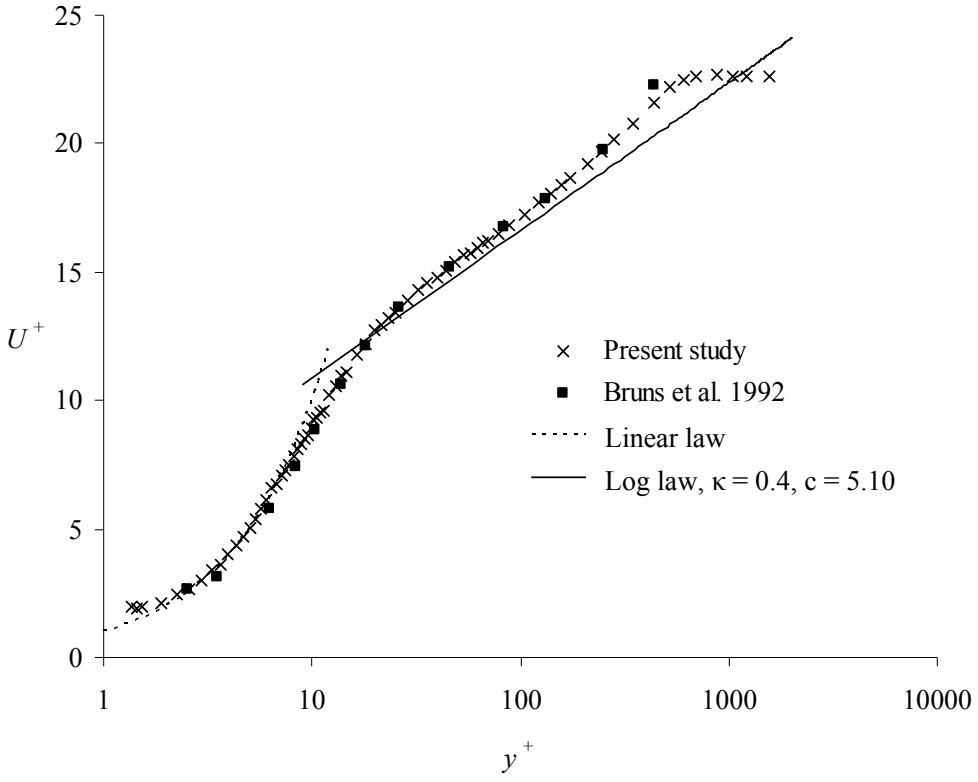

Figure 3.1. Mean velocity profile along test plate.

To determine the streamwise pressure gradient, the streamwise distribution of the streamwise velocity was measured along a line high above the test plate surface representing the free external stream conditions. A height of 200mm above the test plate upper surface was chosen to represent this freestream for the zero-pressure gradient cases. Vertical velocity profile measurements show that the velocity gradients ($\delta u/\delta y$) at these positions were practically zero for the baseline case without blowing and suction. Measurements at the downstream end of the test plate beyond the suction slot showed that the boundary layer thickness was no more than 50mm. Figure 3.2 shows the streamwise velocity distribution over the test plate at y = 200mm. A constant freestream value of about 5.5m/s is observed at all streamwise positions.

The corresponding acceleration parameter,

$$K = \frac{\nu}{U_\infty^2}\frac{dU_\infty}{dx} \tag{3.1}$$

was also calculated and shown in Figure 3.1. Although a streamwise trend exists for the value of K, the magnitudes measured are very small. Patel (1965) shows that for substantial deviation from the log law to occur, K should be greater than 1.6 x 10^{-6}, or about 16 times the value of K measured in the present study. As such, the small pressure gradients measured in this case is considered negligible and the boundary layer may be assumed to behave as one with a zero streamwise pressure gradient, also indicated by the constant freestream velocity measured in the streamwise direction.

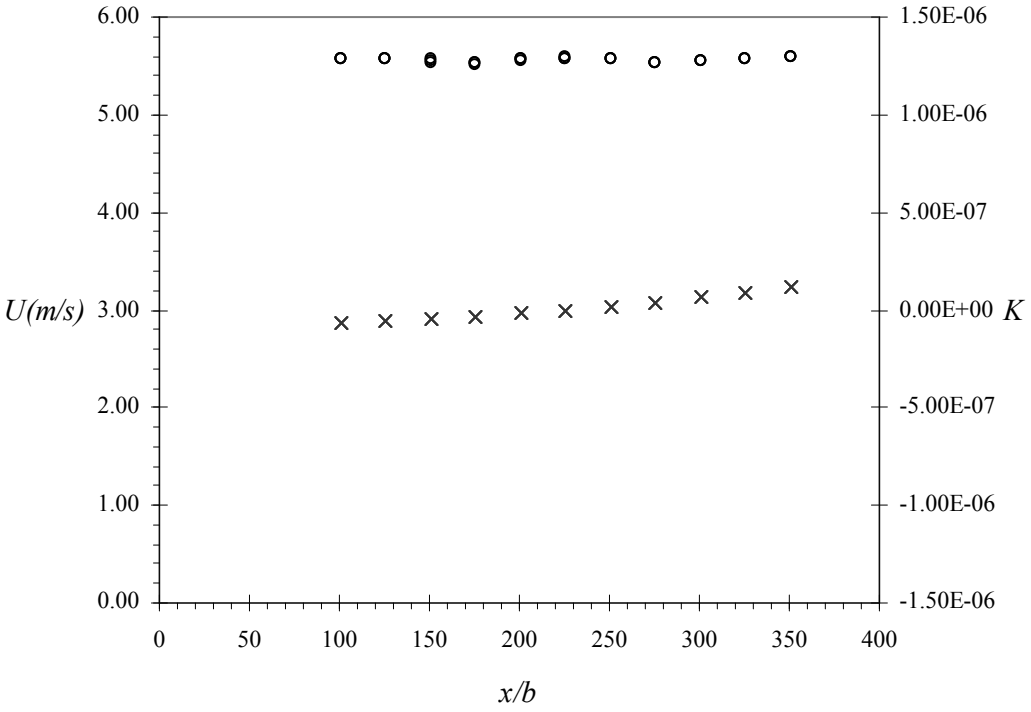

Figure 3.2. Variation of the streamwise velocity (circles) and acceleration parameter K (crosses) in the streamwise direction.

As a further confirmation, static pressure measurements

Of great concern also was the 2-D uniformity of the flow at the blowing and suction slots when they are both activated. Although coarse sponge was fitted into the blowing and suction air plenums to encourage rapid mixing and preliminary measurements at the blowing and suction slots show them to be sufficiently 2-D, further quantitative velocity measurements were carried out over the test plate. Although the uniformity of the jet velocity could be easily determined with the jet issuing from the blowing slot without an external stream, the determination of the uniformity of the suction without an external stream proved much more difficult to measure. This was due to the larger suction slot and multi-directionality of the suction flow with no external stream as mentioned in the previous chapter. It was thus decided that the application of an external flow would allow the uniformity of both

the blowing and suction to be determined most easily. The 2-D uniformity directly downstream of the blowing slot would suggest uniformity of the issuing jet. Similarly, 2-D conditions directly downstream of the suction slot would suggest uniformity of the applied suction.

Figure 3.3 shows the contours of the mean streamwise velocity U measured at x/b = 17, 115, 427 for $0 < y/b < 45$ and $-35 \leq z/b \leq +35$ ($z/b = 0$ being the centerline,) at each streamwise location with the jet exit velocity set at 13.5m/s (Re_j = 1730). The contour lines of the mean streamwise velocity U are equally spaced at magnitude intervals of 0.83m/s for Figure 3.3(a) and 0.25m/s for Figure 3.3(b) and Figure 3.3(c). This difference in contour spacing chosen is due to the very large vertical velocity gradients present near the blowing slot in Figure 3.3(a) where a small velocity magnitude interval results in the contour lines located too closely together. The vertical velocity gradients in Figure 3.3(b) and Figure 3.3(c) were much lower allowing the use of a smaller velocity magnitude interval. The contours show that the flow is close to 2-D over the flat surface. The amount of suction applied was matched to the volume flow rate through the blowing slot.

The coordinate x/b = 17 corresponds to a position just downstream of the blowing slot and x/b = 427 corresponds to a position just downstream of the suction slot. Note that the blowing slot is located at x/b = 0 and suction is applied at x/b = 412. The position x/b = 115 corresponds to a position in between these two slots.

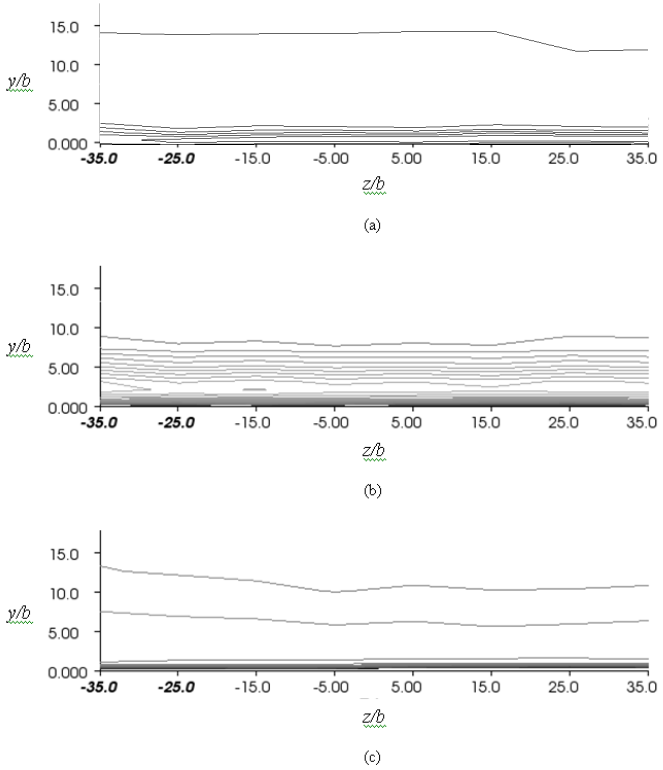

Figure 3.3. Mean velocity U contours measured at various z/b positions. (a): x/b = 17, (b): x/b = 115, (c): x/b = 427.

The plots show that the mean velocity contours are approximately horizontal and parallel to each other at all three x/b positions, indicating reasonably 2-D conditions at these locations. The very close contours in Figure 3.3(a) is due to the narrow high speed jet very close to the wall as it just exits the blowing slot. The near parallel contour lines show the jet to be 2-D. This jet expands upwards and hence lead to the relatively more widely spaced contours observed in Figure 3.3(b). Suction tends to produce a fuller boundary layer directly downstream of it. This is reflected in the contours shown in Figure 3.3(c) where very near the wall, the contours are very closely spaced, but higher above the wall, the contours are much further spread out. Again, the parallel contours show the applied suction to be 2-D. Since the flow is 2-D just downstream of the blowing slot as well as the suction slot, and also 2-D in the

middle portion between them, it may thus be reasonable to assume that the flow is reasonably 2-D over the entire test plate for the measured spanwise locations.

3.1.2. Mean velocity profiles

The mean velocity profiles measured are presented in Figure 3.4 to Figure 3.7 in dimensional form and represent the different stages in the evolution of the wall jet in an external stream with and without suction. Figure 3.4 show the velocity profiles with blowing only in the presence of an external stream for Re_j = 1730, while Figure 3.5 shows the same case but with suction applied.

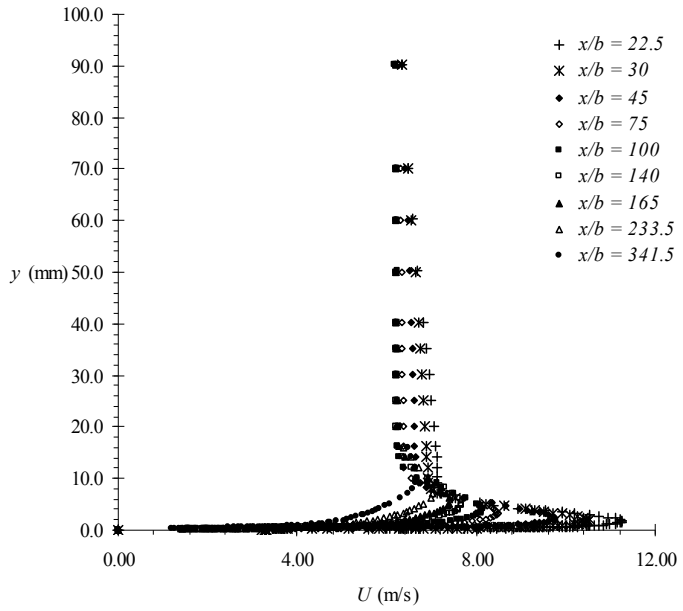

Figure 3.4. Downstream development of the boundary layer velocity profile with blowing and an external stream only with zero pressure gradient, Re_j = 1730.

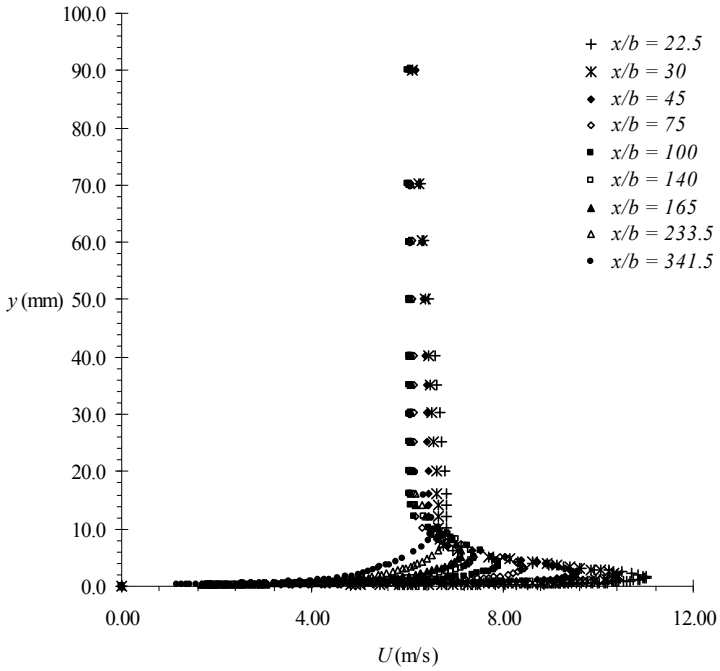

Figure 3.5. Downstream development of the boundary layer velocity profile with blowing, suction and an external stream with zero pressure gradient, Re_j = 1730.

Figure 3.6 and Figure 3.7 further show the mean velocity profiles at the higher jet Reynolds number of 2660 for the cases without and with suction applied respectively.

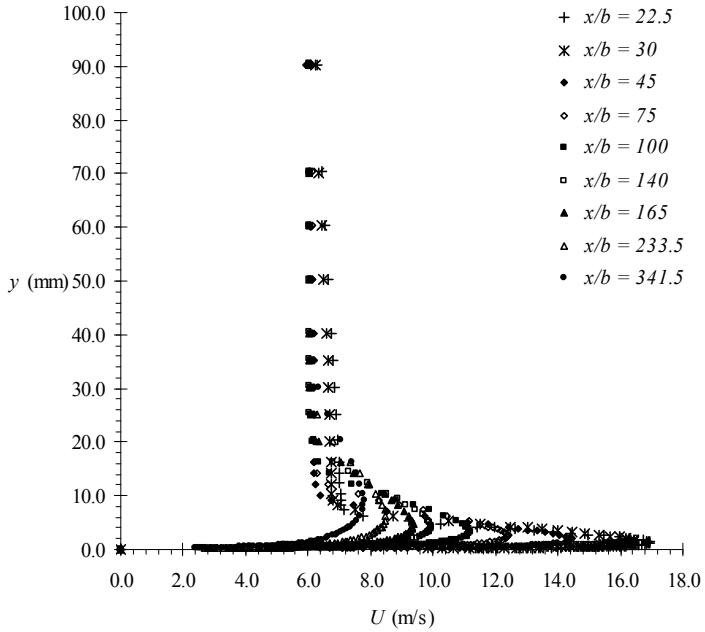

Figure 3.6. Downstream development of the boundary layer velocity profile with blowing and an external stream only with zero pressure gradient, Re_j = 2660.

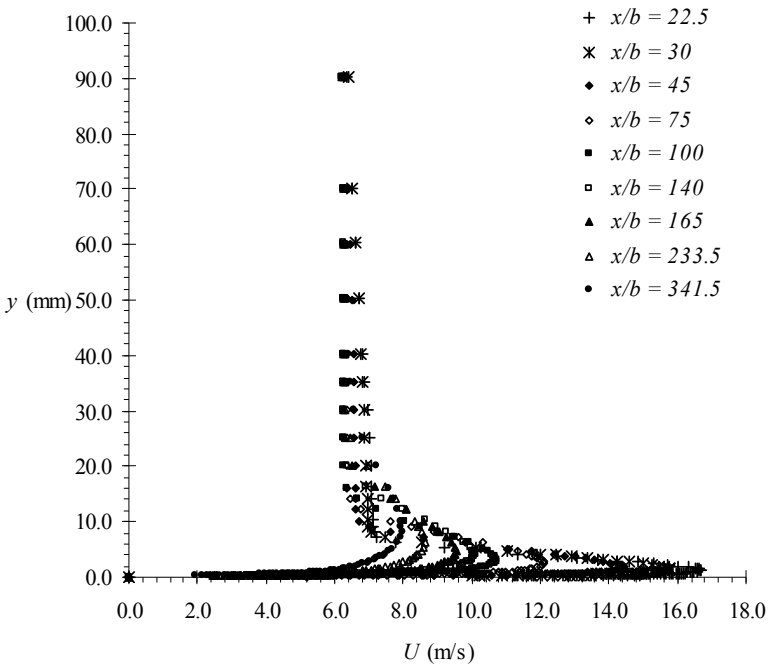

Figure 3.7. Downstream development of the boundary layer velocity profile with blowing, suction and an external stream with zero pressure gradient, Re_j = 2660.

No clear distinction is observed in the profiles at each jet Reynolds number for the case with suction from those without suction, suggesting the minimal effect if any of the suction on the development of the wall jet, at least at the streamwise positions measured.

3.1.3. Similarity of the mean velocity profiles

For laminar flow, the velocity profile in the vertical direction in a boundary layer may be expressed in the form

$$U/U_\infty = f(y/\delta), \tag{3.2}$$

where U is the local velocity, U_∞ is the freestream velocity, y is the vertical coordinate and δ is the boundary layer thickness, which may be taken as the height of

the boundary layer where the local velocity is 99% that of the freestream velocity. This relationship given in equation (3.2) is independent of the streamwise position along the boundary layer and is sometimes referred to as a self-preserving relationship of the flow. Such flows are often called self-preserving flows or self-similar flows, and are said to possess flow similarity.

For turbulent flows such as those encountered in a wall jet, dynamic similarity of the flow requires not only similarity in the mean velocity profile, but also in the profiles of Reynolds stresses and other turbulence quantities (Bradshaw 1976). A general form of the mean velocity and shear stress profiles in a self-similar flow may be given by

$$\frac{U_{ref} - U}{u_0} = F(\frac{y}{l_0}) \tag{3.3}$$

$$-\frac{\overline{uv}}{u_0^2} = g(\frac{y}{l_0}) \tag{3.4}$$

where u_0 and l_0 are the velocity and length scales of the flow, both functions of x and should apply throughout the entire profile.

Although such strict self-similar flows are rarely observed in practice, some types of flows do exhibit a condition of self-similarity in certain regions within the flow. Often the effect of viscosity is small in these regions and the energy containing components of the turbulence is determined by the boundary conditions only. Examples of such flows containing self-similar regions are plane and circular jets, and wakes when observed sufficiently far downstream of their origins.

However in the case of a wall jet, the effect of viscosity cannot be neglected due to very large shear forces present between the rapidly moving jet flow and the stationary

wall just next to it. Studies have shown (Irwin 1973, Zhou and Wygnanski 1993) that for plane wall jets flows without an external stream, precise similarity is impossible. Despite this, many investigators nonetheless have still managed to collapse their wall jet data onto self-similar plots, albeit with different scaling quantities for different portions of the wall jet profile.

With similar intentions to study the applicability of similarity to wall jets with tangential downstream suction in the present study, two velocity scales for the outer and inner regions were defined, similar to those used by Zhou and Wygnanski (1993) in their study of wall jet flow in the presence of an external stream. In the outer region, U_0 is used as a local velocity scale, while the maximum velocity U_m is used as the local velocity scale in the inner region. The physical meanings of these commonly used wall jet notations were presented in Figure 1.2.

An attempt was initially made to employ y_0 as the length scale for both the inner and outer regions. If the scaling quantities were chosen correctly and similarity of the profiles exist, then plotting all the various profiles obtained at the various streamwise locations after scaling with the chosen quantities should yield data points that collapse perfectly onto a single curve. The data plotted in Figure 3.8 and Figure 3.9 for the range of $45 \leq x/b \leq 233.5$ shows that at Re_j of 1730, the data for $y/y_0 < 0.5$ do not collapse using these scales, while Figure 3.10 and Figure 3.11 shows that at Re_j of 2660 the data collapses reasonably well only for $y/y_0 > 0.2$. Below these respective positions, the data scatters within a band of about ± 5%. When both of these cases are superimposed in Figure 3.12, it is clear that both sets of data do not collapse onto each other. Scaling using y/y_0 for both the inner and outer regions thus appears to be

Reynolds number dependent, and in any case has failed to scale the mean velocity profiles appropriately for similarity purposes.

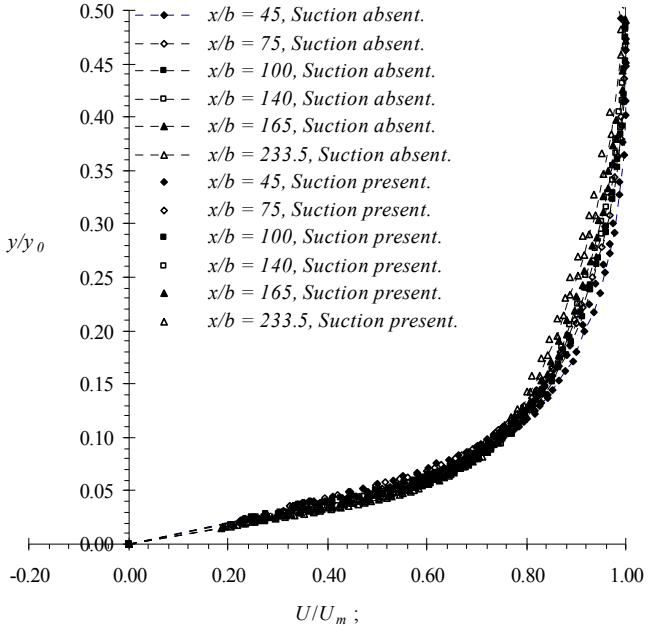

Figure 3.8. Non-dimensionalised inner region velocity profile with blowing and an external stream with zero pressure gradient, Re_j = 1730.

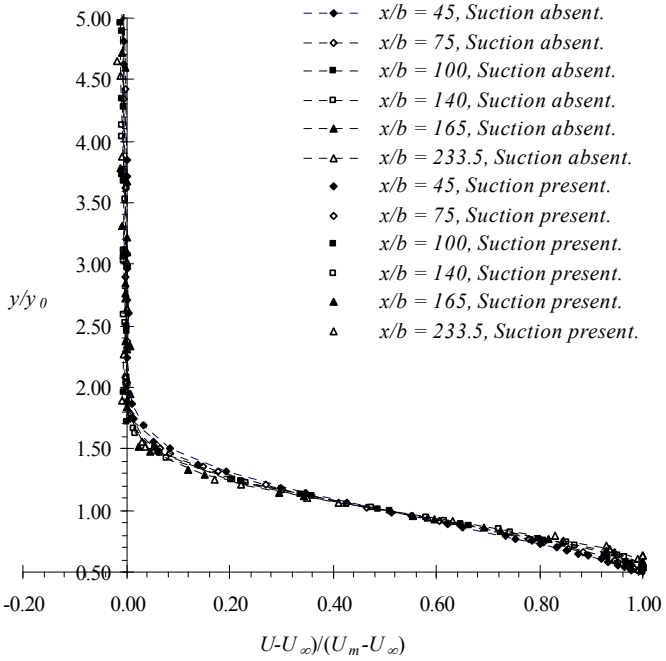

Figure 3.9. Non-dimensionalised outer region velocity profile with blowing and an external stream with zero pressure gradient, Re_j = 1730.

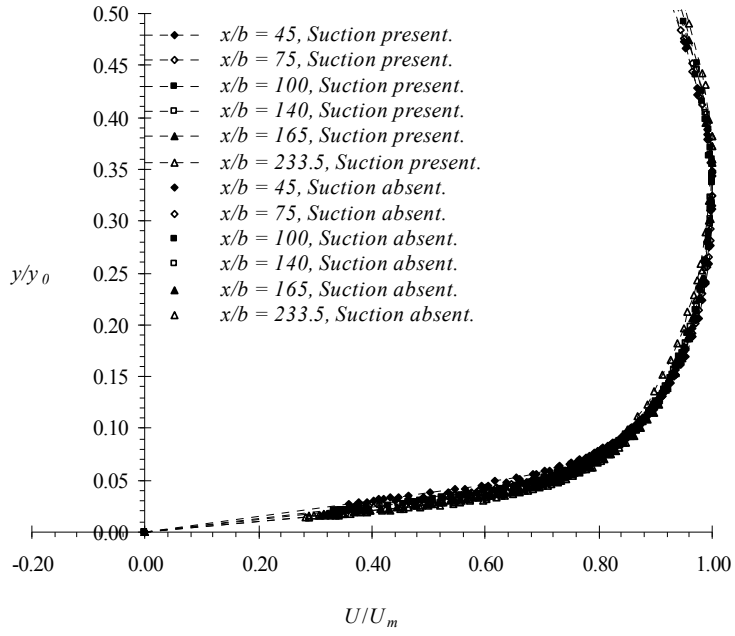

Figure 3.10. Non-dimensionalised inner region velocity profiles with blowing and an external stream with zero pressure gradient, $Re_j = 2660$.

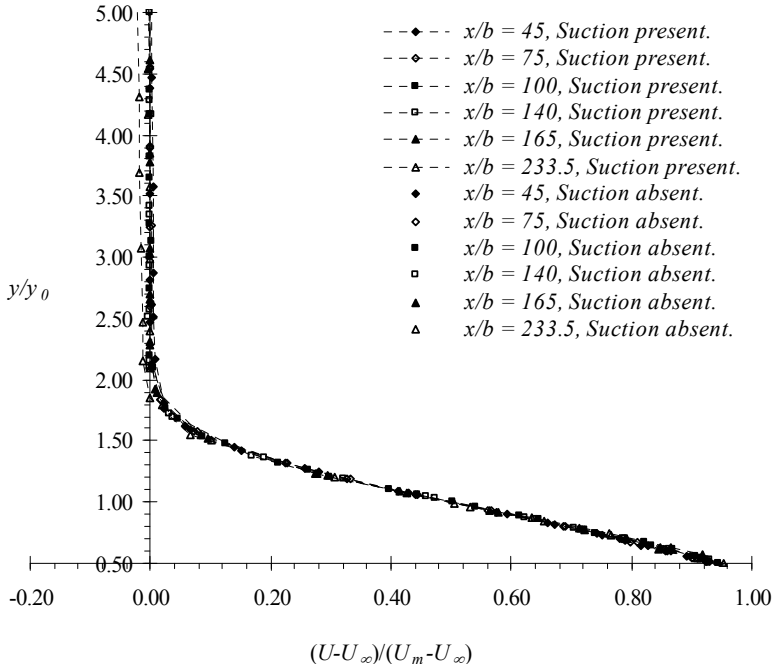

Figure 3.11. Non-dimensionalised outer region velocity profiles with blowing and an external stream with zero pressure gradient, $Re_j = 2660$.

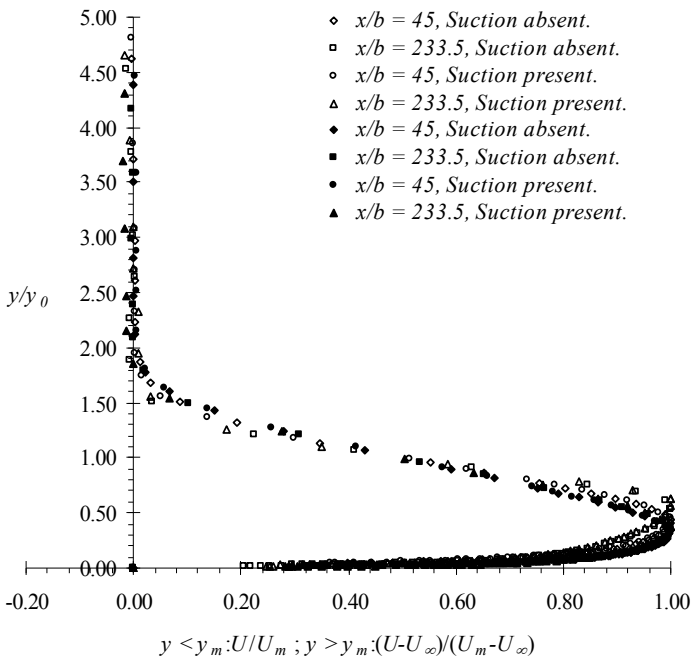

Figure 3.12. Non-dimensionalised velocity profiles with blowing and an external stream with zero pressure gradient. Open symbols: Re_j = 1730, filled symbols: Re_j = 2660.

A further attempt was done using $(U-U_\infty)/U_0$ to scale against a dimensionless distance of $(y-y_m)/(y_0-y_m)$ for the outer region and U/U_m against $(y-y_m)/y_m$ for the inner region (the symbols used are defined in Figure 1.2). Figure 3.13 to Figure 3.16 show the data for the two jet Reynolds numbers of 1730 and 2660 plotted with these scales. They only include data sets where the ratio U_∞/U_m was empirically observed to be less than 0.8 at those locations. The ratio U_∞/U_m is significant as it represents the level of jet decay. As the jet proceeds downstream form the exit nozzle, its local maximum velocity U_m slows down. Since the velocity of the external flow U_∞ is constant for the zero pressure gradient case under consideration, the ratio U_∞/U_m increases gradually as the jet develops downstream. Far downstream, the velocity profile returns to that of a developed boundary layer with $U_\infty/U_m > 1$ and where the effect of the jet on the

mean velocity profile is no longer observable. The ratio U_∞/U_m is minimum at the jet exit, where the local maximum jet velocity is greatest. Somewhere between these two extreme values lies a value of U_∞/U_m where the effect of the jet on the velocity profiles is sufficiently weak that "similarity" is no longer observed. Table 3.1 shows the values of for the various cases at various streamwise distances from the blowing slot.

Table 3.1 Streamwise distribution of U_∞/U_m

x/b	Suction present?	U_∞/U_m	*x/b*	Suction present?	U_∞/U_m
45	No	0.56	45	No	0.38
75	No	0.65	75	No	0.44
100	No	0.68	100	No	0.49
140	No	0.72	140	No	0.55
165	No	0.74	165	No	0.59
233.5	No	0.78	233.5	No	0.65
341.5	No	0.82	341.5	No	0.71
45	Yes	0.58	45	Yes	0.38
75	Yes	0.65	75	Yes	0.45
100	Yes	0.70	100	Yes	0.51
140	Yes	0.74	140	Yes	0.55
165	Yes	0.77	165	Yes	0.58
233.5	Yes	0.82	233.5	Yes	0.64
341.5	Yes	0.84	341.5	Yes	0.69

Zhou and Wygnanski (1993) determined this value of U_∞/U_m to be 0.5 such that above 0.5, the data do not collapse onto each other very well when plotted on self-similar plots. In this study, collapse of the data points was observed at positions where the ratio U_∞/U_m is as high as 0.8, as seen in Figure 3.11 where the same scales as Zhou and Wygnanski's (1993) were used. The range observed in the present study ($U_\infty/U_m \leq 0.8$) includes the smaller range ($U_\infty/U_m \leq 0.5$) proposed by Zhou and Wygnanski (1993), who also noted that the observed self-similarity of the mean

velocity profile does not instantly fail at the proposed threshold. Instead the collapse of the data becomes increasingly poorer as the jet develops downstream and as U_∞/U_m increases. It appears that the threshold value is determined depending how stringent the requirement for data collapse is. Considering that the wall jet flow cannot achieve perfect self-similarity, a judgment needs to be made on what would be considered an acceptable collapse of the data and thus deemed self-similar. It thus appears from the present results that although Zhou and Wygnanski (1993) suggested a value of 0.5 as the threshold for self-similarity to be observed, a value up to 0.8 may also be acceptable, at least for the present range of jet Reynolds numbers.

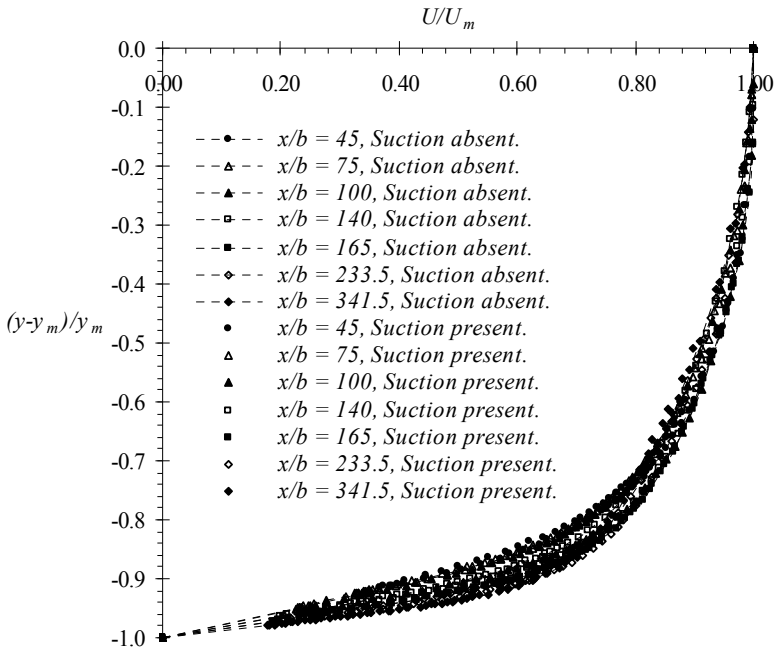

Figure 3.13. Non-dimensionalised inner region velocity profile with blowing and an external stream with zero pressure gradient, Re_j = 1730.

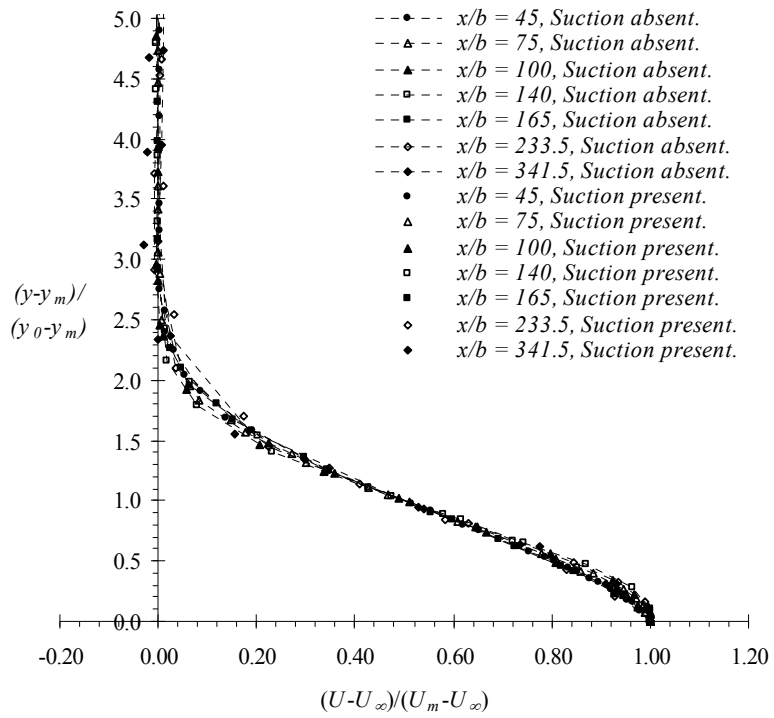

Figure 3.14. Non-dimensionalised outer region velocity profile with blowing and an external stream with zero pressure gradient, Re_j = 1730.

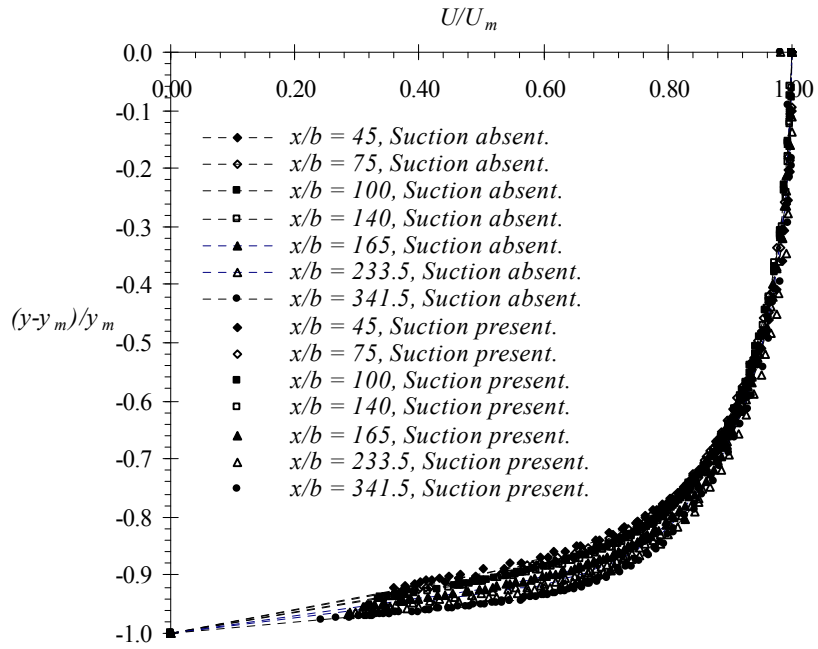

Figure 3.15. Non-dimensionalised inner region velocity profile with blowing and an external stream with zero pressure gradient, Re_j = 2660.

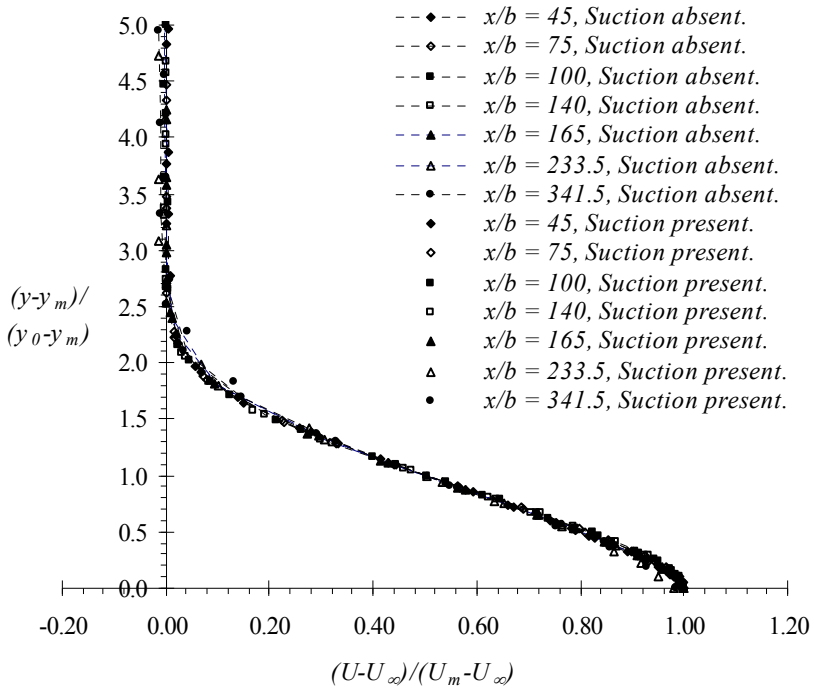

Figure 3.16. Non-dimensionalised outer region velocity profile with blowing and an external stream with zero pressure gradient, $Re_j = 2660$.

When the outer region data sets for both Reynolds number are plotted together as shown in Figure 3.17, they fall onto a single curve, showing that this scaling is independent of the jet Reynolds number. For clarity, only selected sets satisfying the criteria $U_\infty/U_m \leq 0.8$ are plotted in the figure.

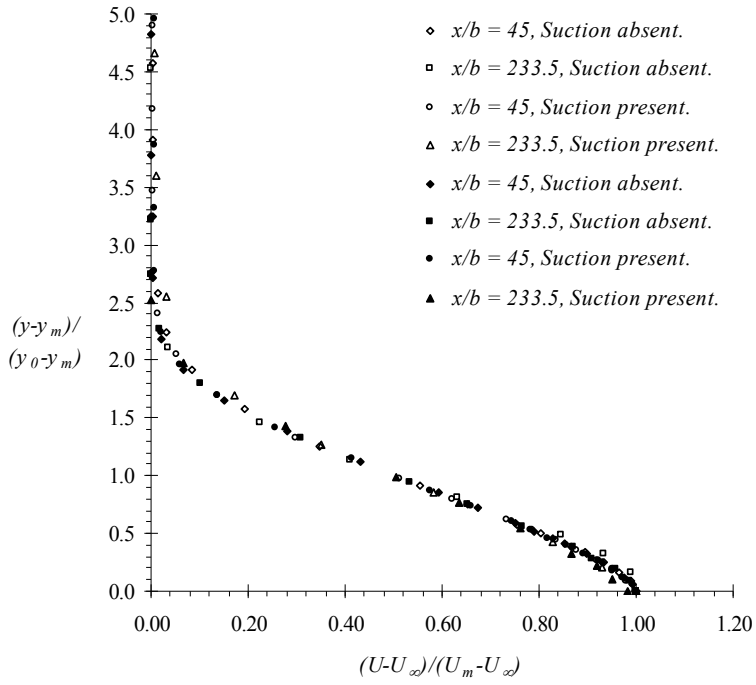

Figure 3.17. Non-dimensionalised outer region velocity profiles with blowing and an external stream with zero pressure gradient. Open symbols: Re_j = 1730, filled symbols: Re_j = 2660.

For the inner regions at both Reynolds numbers, no collapse of the data is observed. Instead, the plots appear to deviate from each other increasingly as the jet progresses downstream such that similarity is not observed for any range of U_∞/U_m values. The deviation is greatest at the lower portions of the velocity profile nearest the solid wall as observed in Figure 3.13 and Figure 3.15.

In view of this poor collapse of the data in the inner region at both jet Reynolds numbers, the mean velocity profiles near the wall were rescaled using the friction velocity U_τ ($U_\tau = \sqrt{\tau_w/\rho}$) to normalize (U-U_m) and plotted against the length scale y/y_0. This length scale is commonly used to scale turbulence intensity profiles for free plane jets (George et al. 2000). In this study, the wall shear stress, or skin friction is determined from the velocity profile measurements very near the wall. The high

resolution of the traverse systems allows very small accurate movements of the probe very near the wall. Figure 3.18 shows the near wall portion of the mean velocity profile for the case with blowing and the external stream only at x/b = 140. Both dimensional as well as non-dimensional (wall based) coordinates are shown.

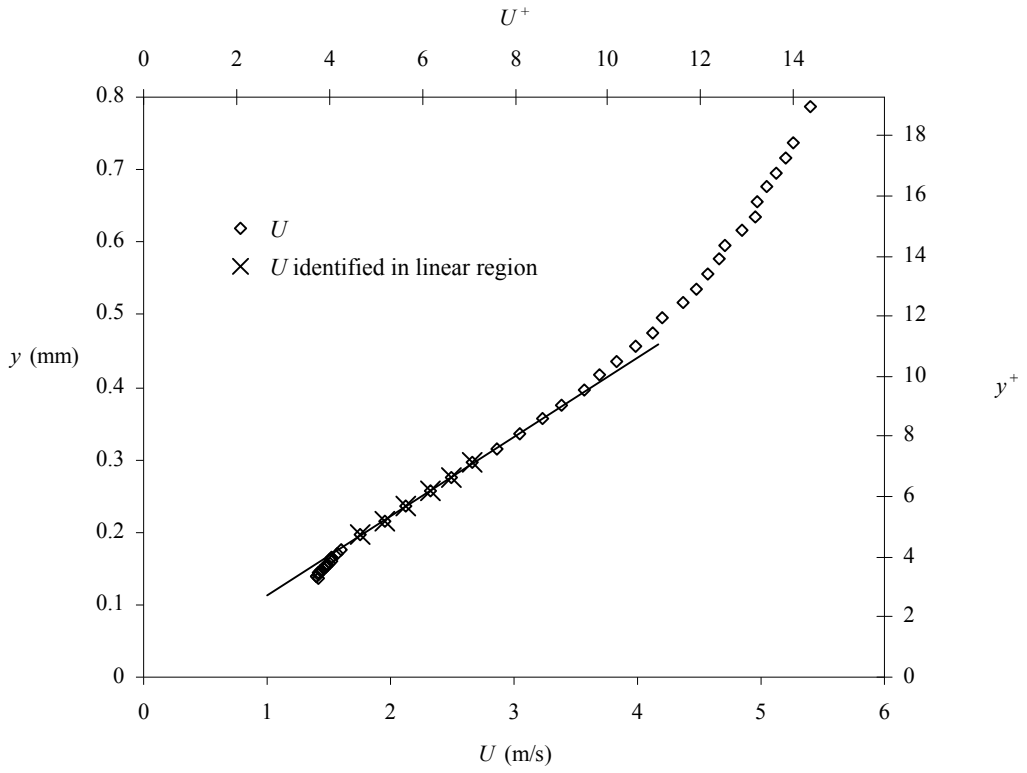

Figure 3.18. Typical measured velocity profile near the wall.

The diamonds in the figure represent measured data points of the mean velocity profile, while the crosses are the points identified as the linear region used for determination of the mean skin friction. The straight line is obtained by linear regression of these identified points. To ensure that the velocity gradient at the wall is accurately determined, at least six points between $3 < y^+ < 7$ (Chew *et al.* 1998, Marineau *et al.* 2006) are used and that the regression coefficient of the line so obtained is at least 0.99 for all the measured positions. Very near the wall, the data

points are observed to curve away from the expected linear trend. This deviation is due to the wall effect (Chew *et. al.* 1998), where conductivity of the solid surface begins to affect the accuracy of the hot-wire measurements. These portions of the measured velocity profiles are recognized as erroneous and neglected in all subsequent considerations.

From the obtained velocity profiles, the velocity gradients at the sub-layer was determined graphically and the mean wall shear stress τ_w as well as the friction velocity u_τ are calculated from it using the following equations:

$$\tau_w = \mu \left. \frac{\delta U}{\delta y} \right|_{wall} \tag{3.5}$$

$$u_\tau = \sqrt{\frac{\tau_w}{\rho}} \tag{3.6}$$

The dimensionless variables U^+ and y^+ shown in Figure 3.18 are then calculated from the friction velocity as follows:

$$U^+ = \frac{U}{u_\tau} \tag{3.7}$$

$$y^+ = \frac{y u_\tau}{\nu} \tag{3.8}$$

This method to estimate the mean wall shear stress is similar to that used by Neuendorf and Wygnanski (1999) for the determination of the wall shear stress. One important advantage of this method over other common indirect methods of skin friction measurements such as surface fences and Preston tubes is that it does not

assume the existence of the "law of the wall", which may be debatable in the present case of a jet boundary layer flow (Patel 1962). It does however assume that the flow is predominantly in the streamwise direction with very small spanwise and vertical components. This assumption is valid for the present case of a 2-D thin wall jet flow, and thus this method is chosen. The use of a Perspex test surface minimizes the conductivity of the wall and thus allows accurate measurements to be made closer to the wall. Figure 3.19 and Figure 3.20 show the inner region velocity profiles for y/y_0, < 0.5 obtained using this new scaling. Note that this scaling uses a inner region parameter to scale the velocity and an outer region parameter to scale the vertical coordinate. This unusual mixed scaling however, allows a better collapse of the near wall data compared to just using inner region parameters or outer region parameters alone. This may suggest that the inner layer structures are closely related to the outer region boundary conditions.

While the data for $Re_j = 2660$ collapses relatively well, the collapse of the corresponding data for $Re_j = 1730$ data is considerably poorer. The greatest deviation from the mean curve occurs in the range $0.1 < y/y_0 < 0.4$.

When both sets of data at the two jet Reynolds numbers are plotted together as shown in Figure 3.21, it is clear that they do not collapse onto each other. Similar to the first scaling used with y_0 for the vertical scale, this scaling using the friction velocity also show a dependency on the jet Reynolds number.

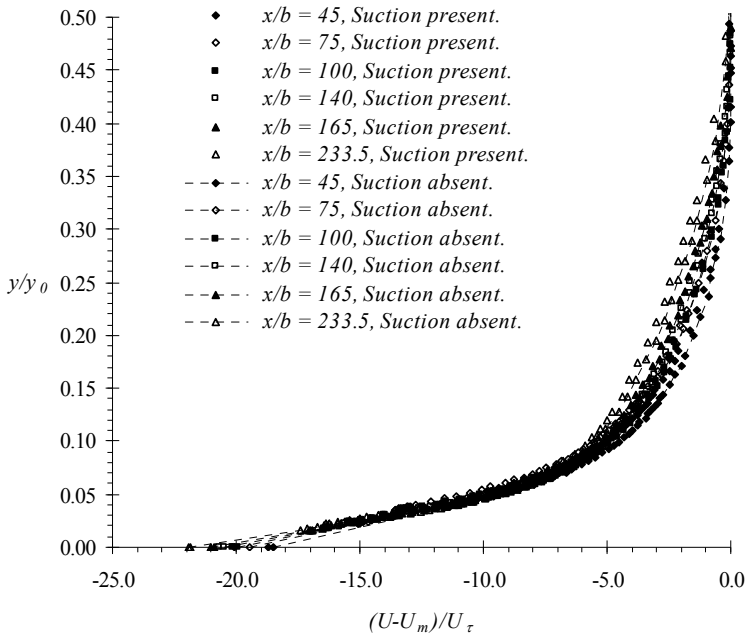

Figure 3.19. Non-dimensionalised inner region velocity profile with blowing and an external stream with zero pressure gradient, Re_j = 1730.

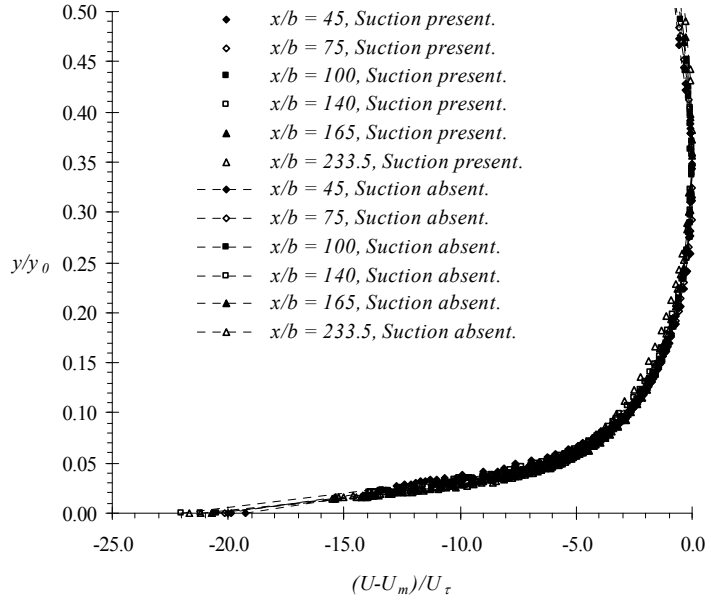

Figure 3.20. Non-dimensionalised inner region velocity profile with blowing and an external stream with zero pressure gradient, Re_j = 2660.

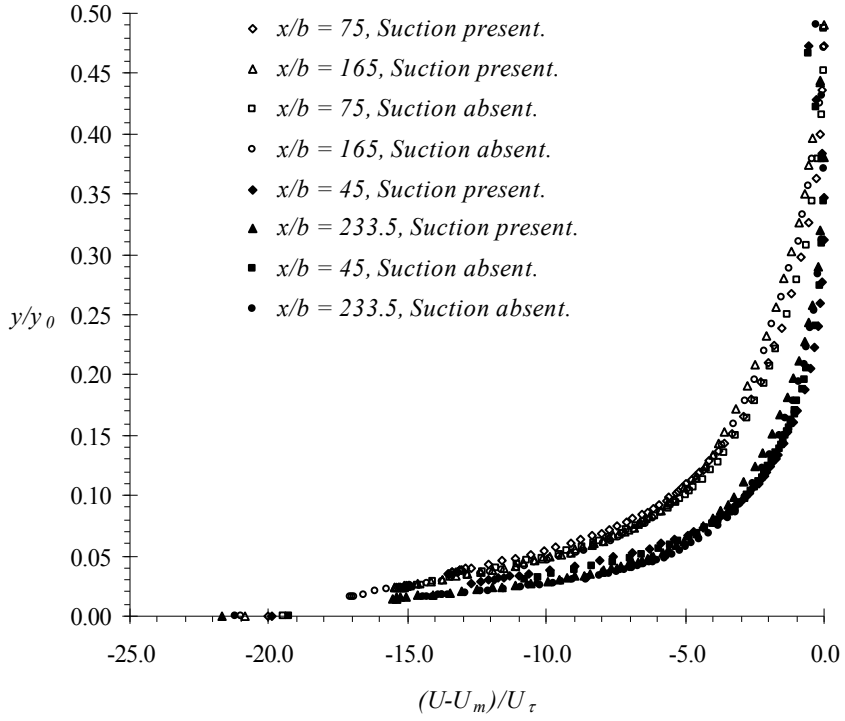

Figure 3.21. Non-dimensionalised inner region velocity profile with blowing and an external stream with zero pressure gradient. Open symbols: Re_j = 1730, filled symbols: Re_j = 2660.

3.1.4. Turbulence intensity profiles

Wygnanski *et al*. (1992) found that even at positions where self-similarity in the mean velocity profiles are observed for a plane wall jet without an external stream, their turbulence intensity profiles still may not exhibit self-similarity. Their measurements of the velocity profiles were made at a distance of up to 120 slots widths downstream of the jet nozzle. While it might be argued that this is insufficient for the flow to reach a state of similarity, they noted that self-similarity of all three components of the turbulence intensity in a free plane jet flow without an external stream is attained at much shorter distances from the nozzle.

An attempt was made to use the same scaling as Wygnanski *et al*. (1992) for the present study where an external stream is present and also at greater distances away from the jet nozzle. The root means square (rms) of u' was normalized by the maximum velocity U_m and plotted against the dimensionless length scale y/y_0. Figure 3.22 and Figure 3.23 show the plots of the turbulence intensity profiles for Re_j of 1730 and 2660 at streamwise positions in the range $45 \leq x/b \leq 341.5$.

Clearly the data do not collapse at all at either jet Reynolds number, similar to the conclusion obtained by Wygnanski *et al*. (1992). This is in spite of measurements being made as far downstream as 340 nozzle widths away from the jet nozzle exit, almost three times the furthest measurement made by Wygnanski *et al*. (1992).

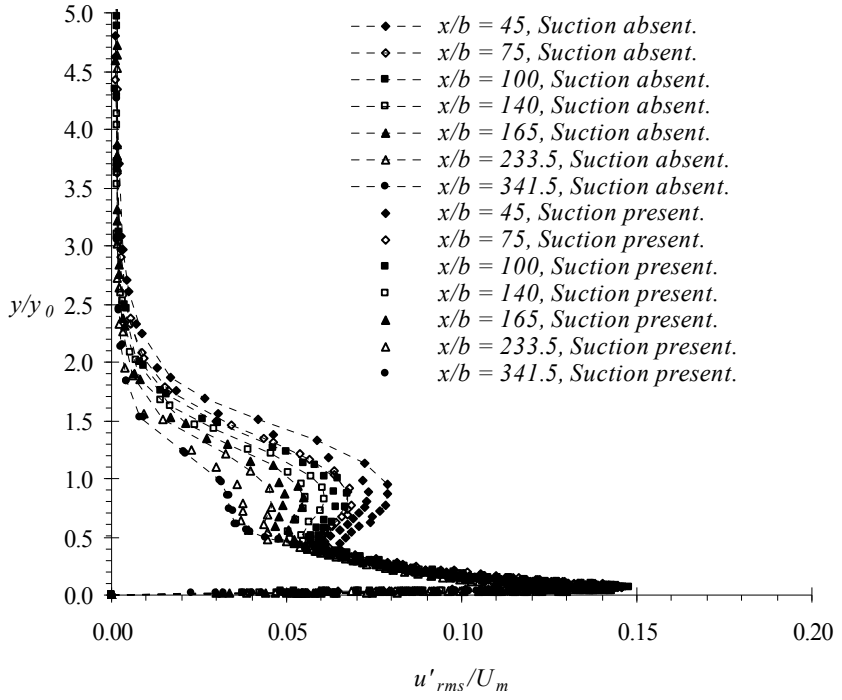

Figure 3.22. Non-dimensionalised turbulence intensity profile with blowing and an external stream with zero pressure gradient, $Re_j = 1730$.

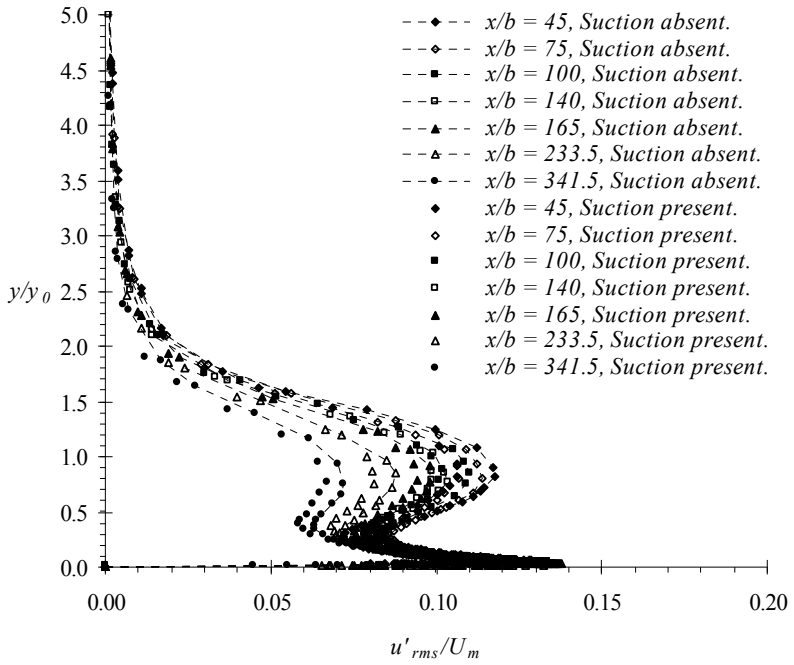

Figure 3.23. Non-dimensionalised turbulence intensity profile with blowing and an external stream with zero pressure gradient, $Re_j = 2660$.

This difference with the plane free jet may be attributed to the lack of equilibrium in the plane wall jet due to the presence of viscous friction with the wall. Wygnanski *et al*. (1992) found that the dependence of u'/U_m on the streamwise location x at the outer part of wall jet flow implies that the wall inhibits the evolution of the large eddies well beyond the location where $U = U_m$.

An interesting observation from both Figure 3.22 and Figure 3.23 is that the turbulence intensity of the wall jet flow reduces in the presence of the suction at both jet Reynolds numbers studied. This is somewhat similar to Park and Choi's (1999) results where normal wall suction was found to reduce the turbulent intensity above the wall at the suction position. The present result indicates that the presence of

tangential suction downstream stabilizes the flow even far upstream of the suction slot.

A much improved collapse of the data is obtained if the turbulence intensities are scaled using the value of u'_{rms} at $y = y_0$. Figure 3.24 and Figure 3.25 show this new scaling plotted against y/y_0 for the two jet Reynolds numbers.

A significant improvement in the collapse of the data is observed for positions $y/y_0 \geq 0.5$. Although some scatter (within a band of about ±5%) is observed in the shear flow region above the position of maximum jet velocity at around $y/y_0 = 1$ for $Re_j = 1730$, the collapse at $Re_j = 2660$ for $y/y_0 \geq 0.5$ is surprisingly good. The data for the cases with and without suction appear to collapse onto each other at each jet Reynolds number. Using this scaling, the largest deviations in the data also occur near the solid surface where the production of turbulent energy is the highest due to viscous friction and this may possibly hamper the development of equilibrium conditions.

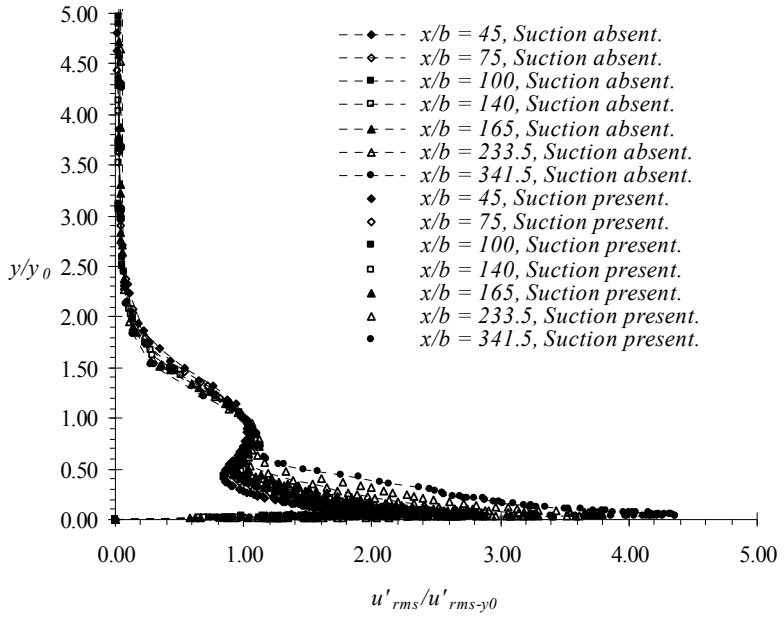

Figure 3.24. Non-dimensionalised turbulence intensity profile with blowing and an external stream with zero pressure gradient, $Re_j = 1730$.

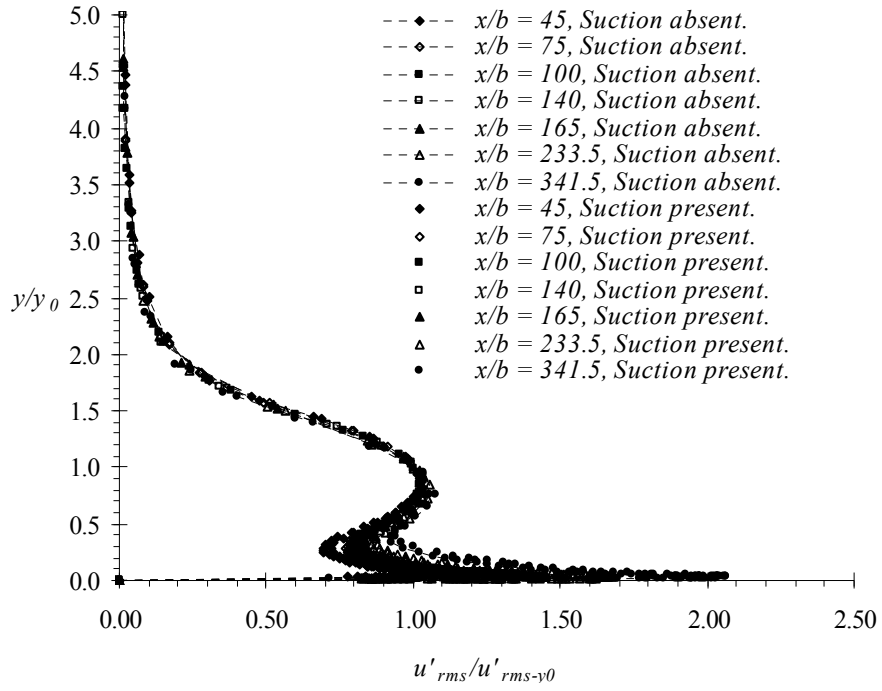

Figure 3.25. Non-dimensionalised turbulence intensity profile with blowing and an external stream with zero pressure gradient, $Re_j = 2660$.

This effect of viscous friction is observed not only in the turbulence intensity distributions but also in the mean velocity distribution as shown in Figure 3.13 and Figure 3.15 at the lower regions of the velocity profiles near the wall. Increasing the jet Reynolds number from 1730 to 2660 shows a marked improvement in the collapse of both the mean velocity as well as the turbulence intensity data. This point is also clearly observed by comparing Figure 3.14 with Figure 3.16, and Figure 3.19 with Figure 3.20. In all these cases, the higher jet Reynolds number case shows a better collapse of the respective data compared to the corresponding lower jet Reynolds number case. This again suggests viscous effects hampering equilibrium conditions from developing and resulting in poorly collapsed data.

3.2. Adverse pressure gradient case

To study the effect of an adverse pressure gradient on the development of a wall jet flow in the presence of an external stream and suction, the flat plate model shown in Figure 2.1 was installed at an inclination of about 15° to create a diverging test section above the flat inclined surface. This was easily done as the plate could be rotated about a pivot point located at the center of curvature of the leading edge radius. At this inclination angle, the flow separates near the leading edge and forms a separation bubble over the entire streamwise length of the inclined plate. This relatively large angle was chosen to better simulate the kind of flow over an aircraft wing in the post-stall regime, where the flow above the wing is separated in the absence of any flow control devices. The flow was visualized using tuff, repeated three times over a period of time. The patterns so obtained were consistent and repeatable, showing that the separation bubble that forms over the test plate with the imposed adverse pressure gradient is stable. Figure 3.26 is the result of superimposing over a hundred individual tuft visualization photographs and shows the extent of this separation bubble. Apart from the flow separation over the test surface, no separation is observed at the roof or side walls of the wind tunnel. Since an area of reverse flow is present within the separation bubble, and the hot-wire probe is unable to determine flow direction, quantitative hot-wire data is not acquired for this case of an adverse pressure gradient without blowing and suction.

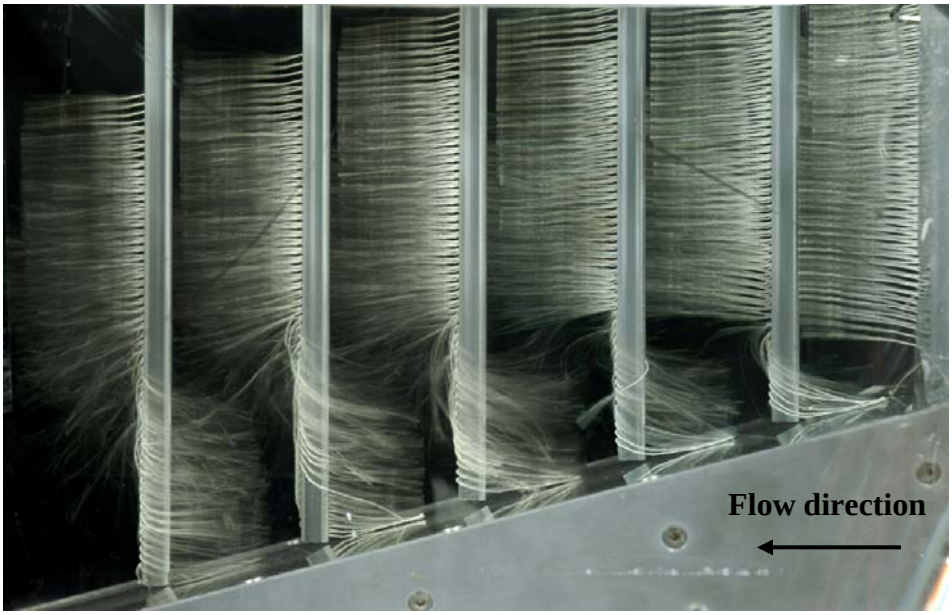

Figure 3.26. Tuff visualization for adverse pressure gradient case with no blowing and no suction.

For this case with an adverse streamwise pressure gradient, only the case with the higher jet velocity of 21m/s is studied. Although attached flow is observed for both the jet velocities mentioned previously, the higher velocity jet was chosen for its higher jet Reynolds number. A higher jet Reynolds number would be more applicable to possible field applications such as flow control over an aircraft wing or over the walls of a submarine. The subsequent results and discussions concerning a jet in an adverse pressure gradient only relates to the case with the higher jet Reynolds number of 2660.

Attached flow over the inclined surface of the plate is shown in the tuft visualization result in Figure 3.27 when blowing is applied at Re_j of 2660. Because the flow is attached, no separation bubble is observed under this condition over the whole length of the plate, even downstream of the suction slot.

Figure 3.27. Tuff visualization for adverse pressure gradient case with blowing, Re_j = 2660.

The streamwise mean velocity distributions and the corresponding acceleration parameter K is shown in Figure 3.28. A region where K is relatively constant is observed at the positions $100 < x/b < 400$.

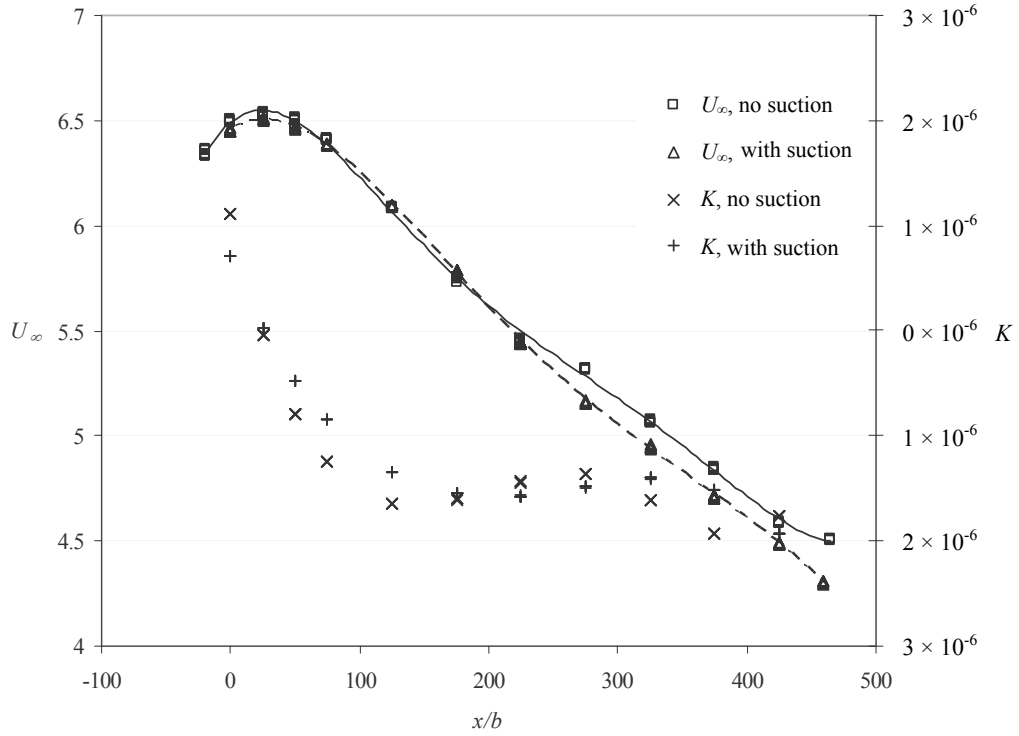

Figure 3.28. Streamwise velocity and acceleration parameter K distribution of the flow above the test plate with blowing and an external stream, $Re_j = 2660$.

The streamwise velocity distributions are similar whether suction is present or not. The absence of flow separation allows quantitative measurements to be made using the hot-wire to study the effect of the adverse pressure gradient to the self-similarity of the wall jet flow in the presence of an external stream and suction. With a jet Reynolds of 2660, the resulting jet velocity ratio U_j/U_∞ is about four at the leading edge over the position of the blowing slot.

3.2.1. Mean velocity profiles

The mean velocity profiles measured in the presence of the adverse pressure gradient are presented in dimensional form in Figure 3.29 for the various streamwise positions.

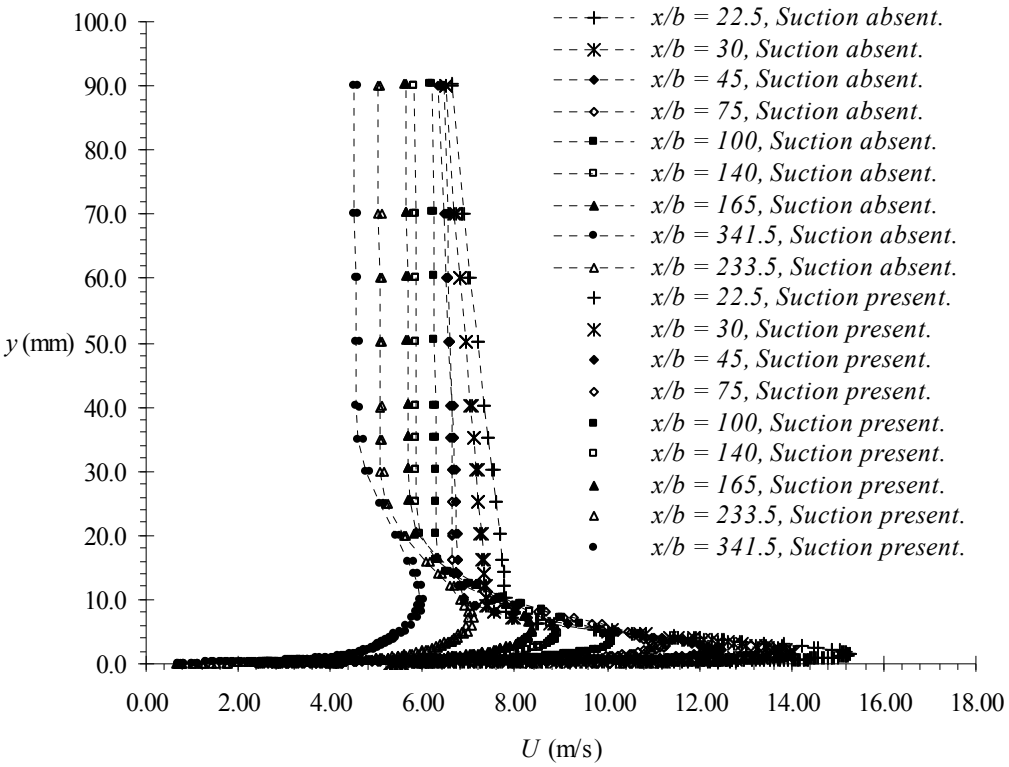

Figure 3.29. Downstream development of the boundary layer velocity profile with blowing, suction and an external stream with an adverse pressure gradient, Re_j = 2660.

The results show the downstream evolution of the flow with an adverse pressure gradient and are similar to that at zero pressure gradient, except for the freestream velocity above the wall decreasing in the downstream direction. The effect of the suction is similarly found to be insignificant at these measured locations.

3.2.2. Self-similarity of mean velocity profiles with an adverse pressure gradient

The jet flow in this adverse pressure gradient case is initially treated similarly with the zero pressure gradient cases. Two regions are similarly identified, the inner region and the outer region and two different length scales (y_0-y_m) and y_m are used to scale each region respectively. The velocity scale used remains the same with that used earlier for the zero pressure gradient case. Figure 3.30 and Figure 3.31 show that these scaling allow the scaled mean velocity profiles to collapse relatively well with each other, particularly for the outer region.

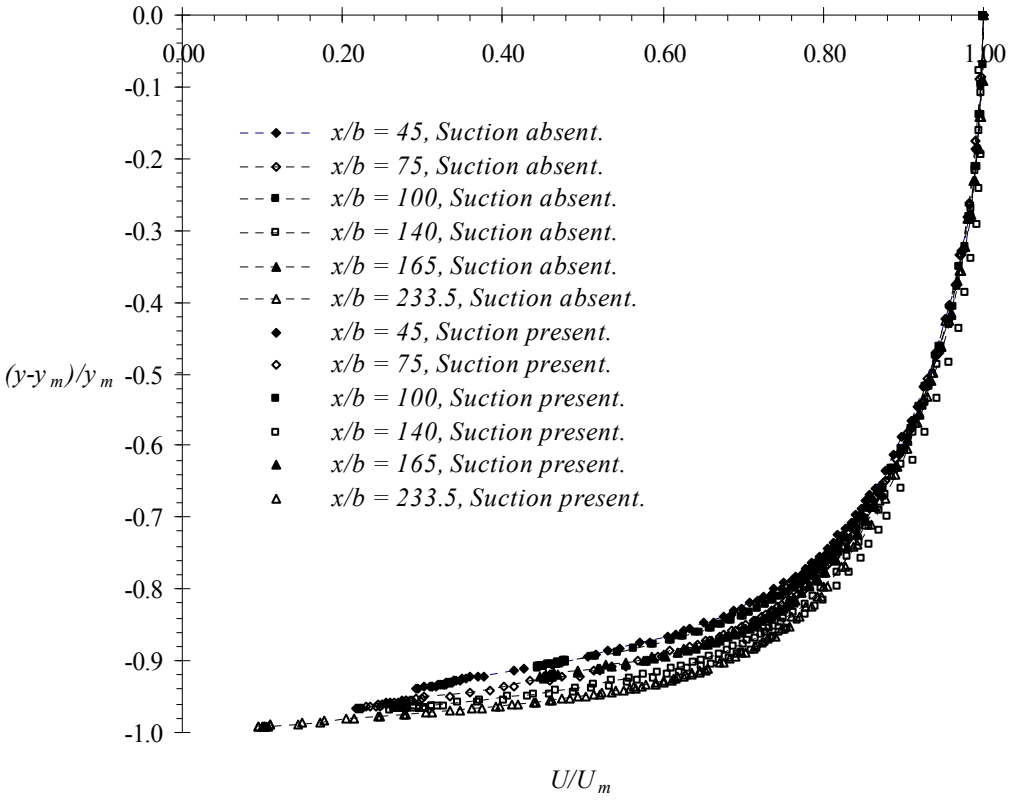

Figure 3.30. Non-dimensionalised inner region velocity profile with blowing and an external stream with an adverse pressure gradient, Re_j = 2660.

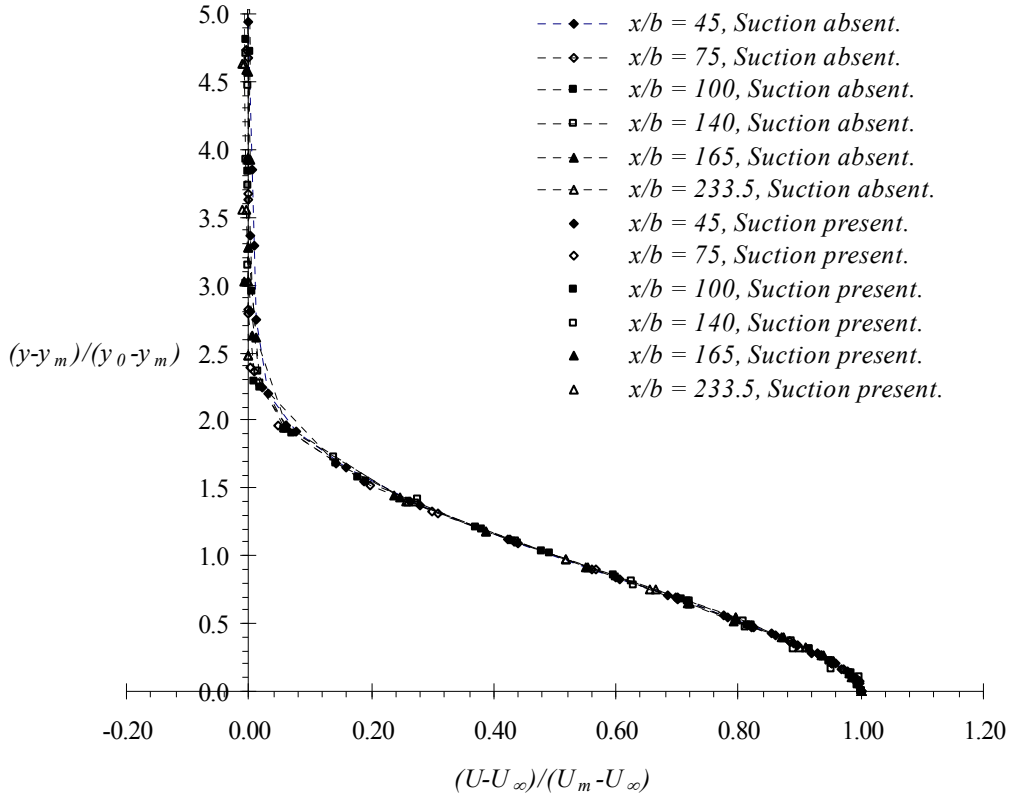

Figure 3.31. Non-dimensionalised outer region velocity profile with blowing and an external stream with an adverse pressure gradient, $Re_j = 2660$.

The inner region shows some scatter in the data within a band of about ±5% for $(y-y_m)/y_m < -0.6$. The greatest scatter is again observed in the region closest to the wall. Comparing these results with Figure 3.15 and Figure 3.16 show that the adverse pressure gradient has reduced the amount of scatter slightly for both for the outer and inner regions. It appears that the adverse pressure gradient is more conducive for self-similarity.

This is similarly concluded by Irwin (1973) in his analysis of the wall jet with an external stream, but without suction. He shows that an adverse pressure gradient, suitably tailored can result in a wall jet flow with an external stream to be self-

preserving. With the aid of Newman's (1967) analysis where skin friction is ignored, Irwin (1973) concluded that for a self-preserving wall jet with an external stream,

$$y_0 \propto (x + x_0) \tag{3.9}$$

$$U_\infty \propto (x + x_0)^m \tag{3.10}$$

where x_0 is the distance of the hypothetical origin upstream from the blowing slot, the exponent m depends on the ratio U_0/U_∞, and y_0, U_0 and U_∞ have the usual meanings defined in Figure 1.2.

Figure 3.32 shows the relationship between y_0 and x for the present study.

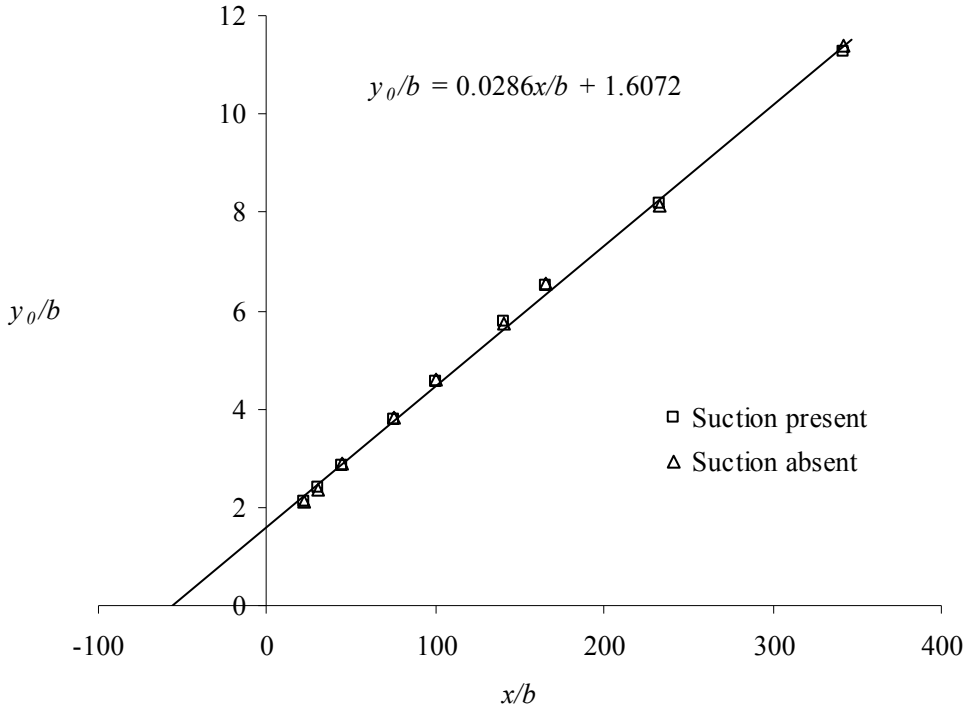

Figure 3.32. Downstream distribution of y_0 along the test plate with an adverse pressure gradient, $Re_j = 2660$.

From the linear regression line shown in Figure 3.32, the value of x_0 is easily calculated as 112mm. The value of m can be calculated from the regression line shown in Figure 3.33 as -0.30.

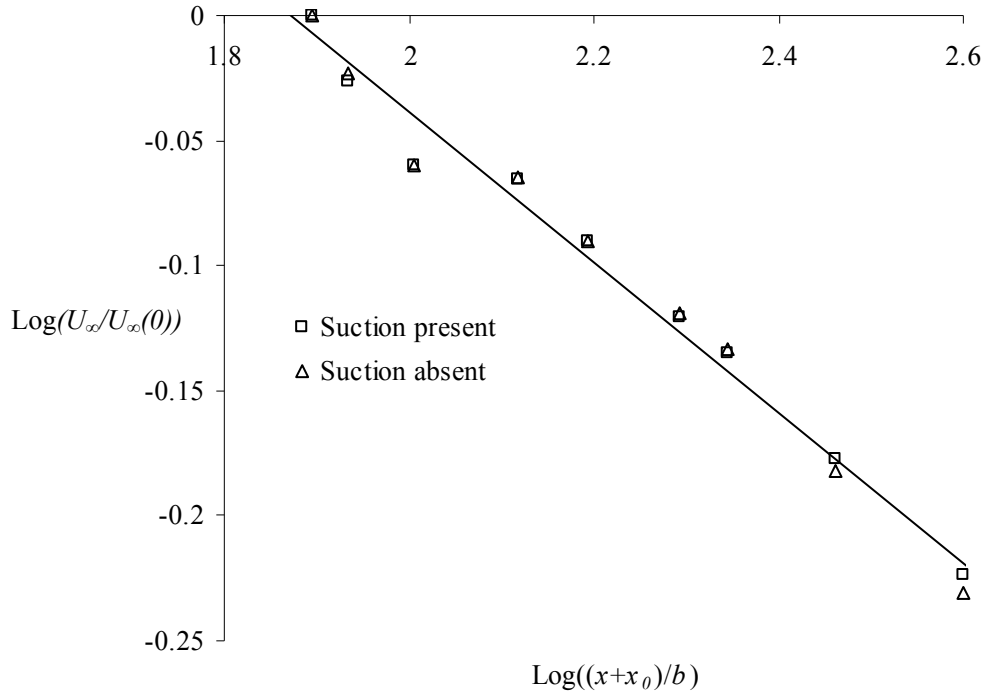

Figure 3.33. Downstream distribution of U_∞ along the test plate with an adverse pressure gradient, Re_j = 2660.

According to these two plots and the criteria specified by Irwin (1973), the jet flow should be self-preserving. The fact that suction is present downstream does not seem to affect the flow in any significant manner with the imposed adverse pressure gradient. While Irwin (1973) specially tailored the distribution of the external stream velocity U_∞ to achieve self-similar flow conditions in his study using adjustable louvres, no such effort to tailor the flow is made in the present study. The adverse pressure gradient was created only by inclining the pivoting test plate. It is interesting

to note that this is sufficient to create conditions conducive for self-similarity even though that was not the specific intention in this study. This self-preservation of the jet is certainly suggested by Figure 3.31 and Figure 3.38, at least for the outer region of the jet. Figure 3.38 however, also suggests some deviation from self-similarity for the inner region of the jet. Irwin suggests using the scaling shown in Figure 3.31 for the outer region also for the inner region. However, when the present results are scaled in this manner as shown in Figure 3.34, the collapse in the data is even poorer than that in Figure 3.30 using y_m and U_m as scaling factors.

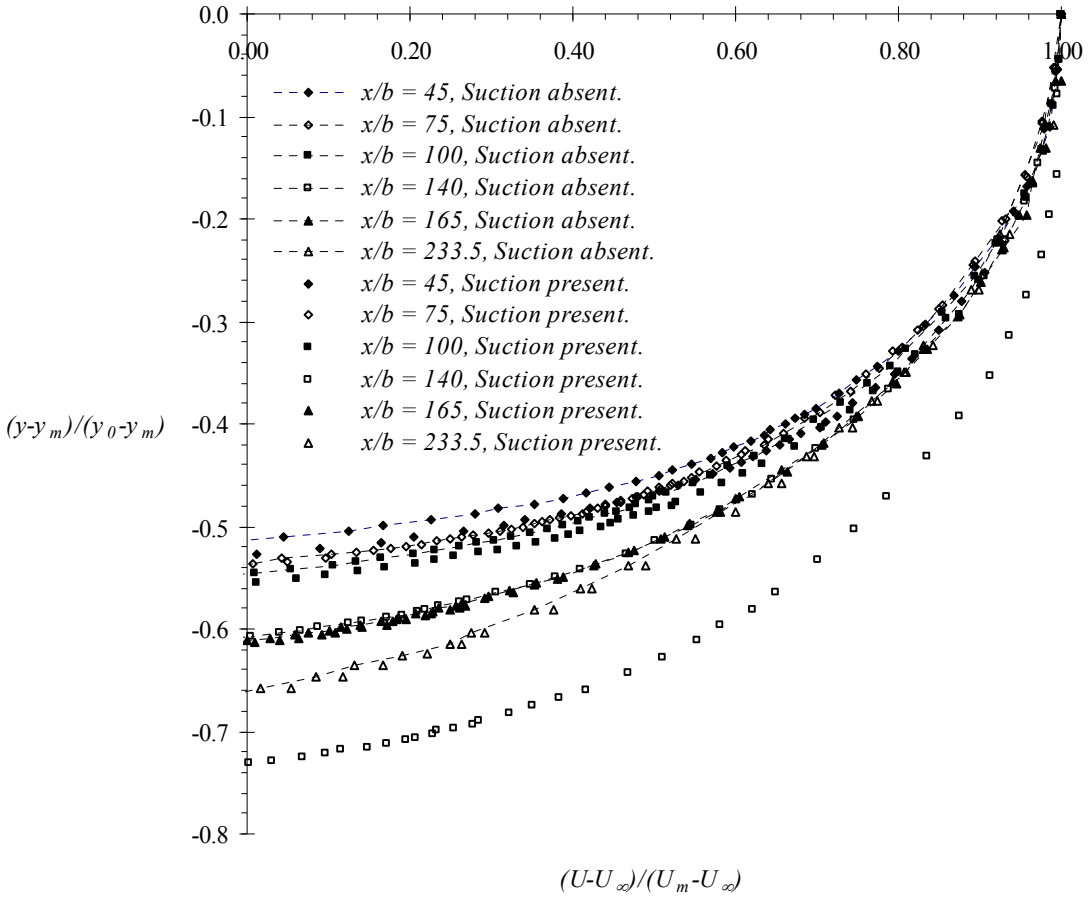

Figure 3.34. Non-dimensionalised inner region velocity profile with blowing and an external stream with an adverse pressure gradient, Re_j = 2660.

Considering the difference in the data collapse in the outer and inner regions following Irwin's (1973) analysis, it is most likely the poor collapse in the inner region is due to breakdown of the assumption that skin friction can be ignored. Near the wall, viscous effects become significant and this assumption becomes invalid, and self-similarity is no longer observed. Irwin (1973) also notes that the analysis holds only if u_τ/U_∞ is constant, but admits that this value usually decreases slightly with increasing x in practice. This is also evident in Figure 3.35 for the present study.

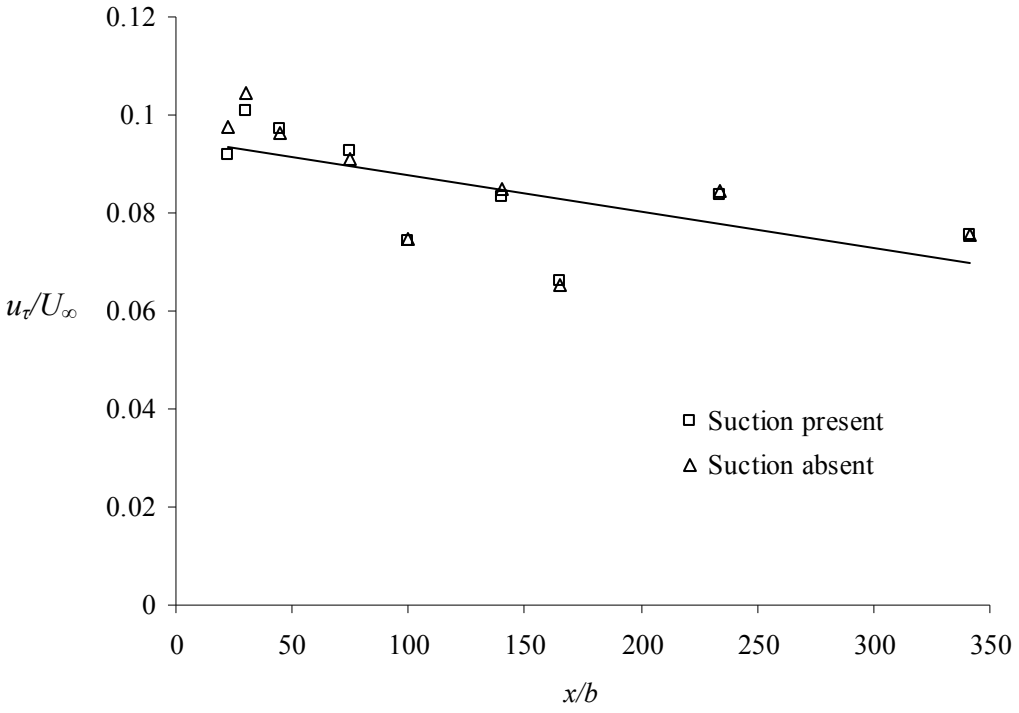

Figure 3.35. Downstream distribution of the friction velocity along the test plate with an adverse pressure gradient, $Re_j = 2660$.

The relatively large amount of scatter in Figure 3.35 is likely due to the difficulty in determining the skin friction at the wall accurately, but is sufficient to show the general trend of the streamwise skin friction distribution along the test plate.

Although the analysis presented by Irwin's (1973) fails in the near wall region, it nevertheless remains useful in predicting the velocity profiles in the outer region.

3.2.3. Similarity of the turbulence profiles

The turbulence intensity profiles are shown in Figure 3.36 and Figure 3.37, scaled using U_m, the local maximum jet velocity. Unlike the cases with zero pressure gradients, the effect of suction on the turbulence intensities in the presence of an adverse pressure gradient is insignificant. The turbulence intensity distributions with suction are practically the same as that without suction at each of the measured locations. The stabilizing effect of suction on the upstream flow appears to be inhibited by the adverse pressure gradient. The lack of collapse also show a lack of flow similarity when the turbulence intensities are scaled in this manner.

Irwin (1973) suggests using U_0 as defined in Figure 1.2 to scale the root mean square of the velocity fluctuations, together with y_0 to scale the vertical coordinate. Using these scales, the plot shown in Figure 3.37 is obtained. Surprisingly, despite the relatively good collapse of the mean velocity data arising from Irwin's (1973) analysis, very poor collapse of the turbulence data is observed at positions below about $y/y_0 \approx 1.5$. A deviation below this y/y_0 value is also similarly observed in Irwin's (1973) results.

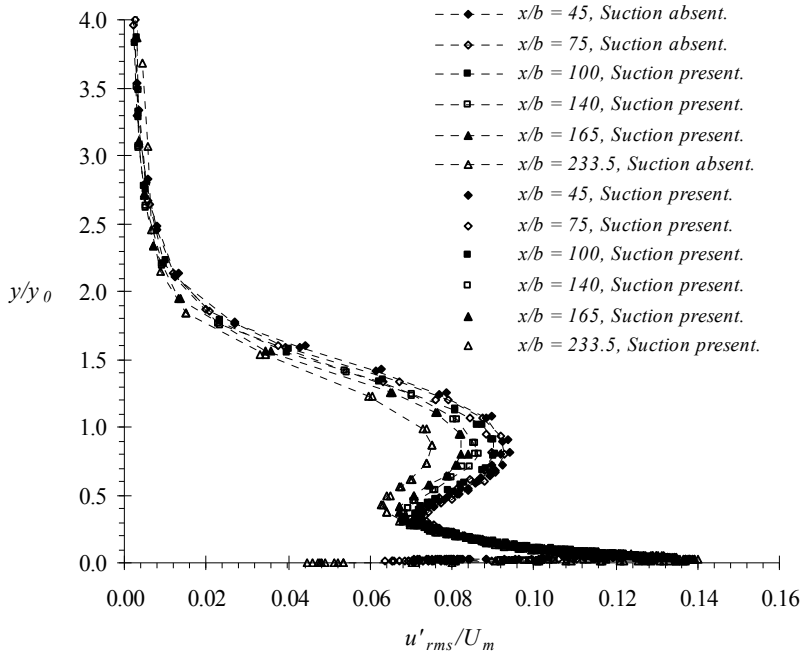

Figure 3.36. Non-dimensionalised turbulence intensity profile with blowing and an external stream with an adverse pressure gradient, $Re_j = 2660$.

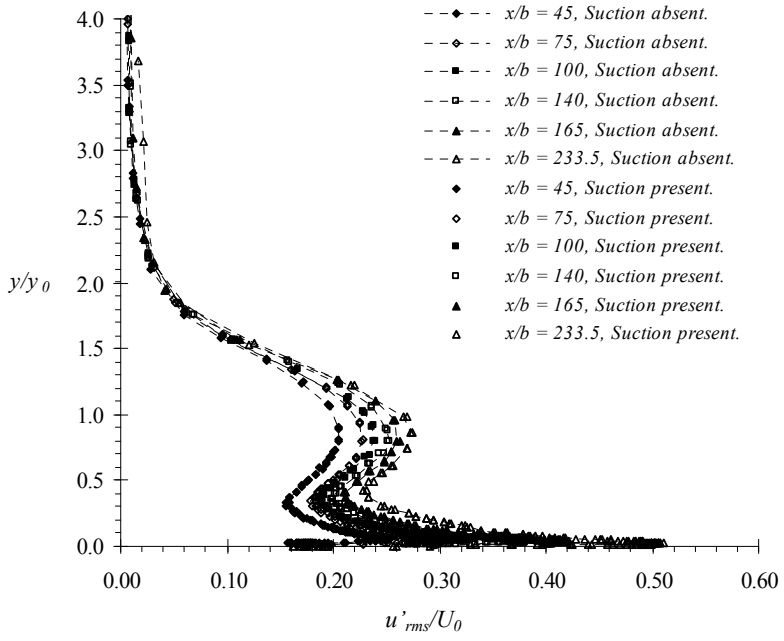

Figure 3.37. Non-dimensionalised turbulence intensity profile with blowing and an external stream with an adverse pressure gradient, $Re_j = 2660$.

Scaling the velocity fluctuations as before in Figure 3.25 however, results in a much better collapse of the data. Figure 3.38 shows the resulting plot when scaled this way. Here the root mean square of the velocity fluctuations is scaled using its value at $y = y_0$. The result shows a very good collapse of the data for positions $y/y_0 > 0.4$, and this is again a slightly wider region of data collapse than for the zero pressure gradient case with $Re_j = 2660$ shown in Figure 3.25.

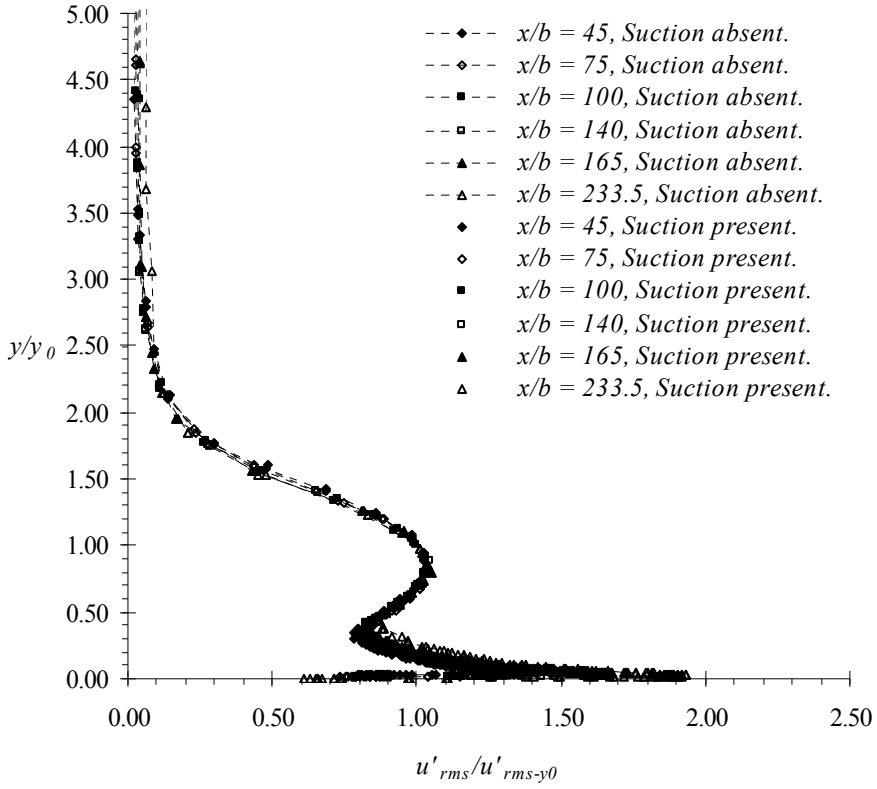

Figure 3.38. Non-dimensionalised turbulence intensity profile with blowing and an external stream with an adverse pressure gradient, $Re_j = 2660$.

The data suggests that the imposed adverse pressure gradient is indeed more conducive for self-similarity of the flow when compared to the zero pressure gradient cases. Self-similarity of both the mean and turbulence profiles is practically observed

in the outer region of the wall jet flow. Suction downstream of the jet with an adverse pressure gradient along the external stream affects the flow insignificantly according to the results. Only very near the wall does self-similarity breaks down, similar to what has been consistently observed for the zero pressure gradient cases and is likely caused by the significant viscous friction present at the wall.

3.3. Parameter scaling of the flow

Narasimha *et al*.(1973) suggest that a fully developed wall jet flow without the presence of an external stream should attain a local equilibrium that is independent of specific nozzle conditions. Its initial kinematic momentum flux is the parameter that determines the evolution of such an incompressible flow for a fluid of a given viscosity. However, for a wall jet in the presence of an external stream Zhou and Wygnanski(1993) suggests that a more appropriate parameter governing the flow in this case is the excess of kinematic momentum flux (J) near the nozzle given by:

$$J = \int_0^\infty (U - U_\infty) U . dy = b(U_j - U_\infty) U_j - U_\infty^2 \theta_0 \tag{3.11}$$

Since the present study shows the effect of suction on the development of a wall jet mean velocities in the presence of an external stream to be minimal over most of the flow, the method used by Zhou and Wygnanski (1993) is adopted to analyze the parameter scaling of the flow.

Since the momentum deficit in the upstream boundary layer θ_0 is negligible in comparison with the excess momentum flux of the jet, the last term in Eq. (3.11) can be omitted. A dimensionless streamwise distance ξ given by

$$\xi = \frac{xJ}{\nu^2} = \frac{x.b(U_j - U_\infty)U_j}{\nu^2} \tag{3.12}$$

and a dimensionless velocity ratio parameter R defined by

$$R = (U_j - U_\infty)/(U_j + U_\infty) \tag{3.13}$$

are used to describe the streamwise evolution of the wall jet flow.

The correlations between these three parameters J, ξ and R with the three most important parameters in a wall jet, y_0, U_m and τ_w are then evaluated. This should result in plots that are independent of jet Reynolds number as well as facilitate the evaluation of τ_w from the mean momentum equation (Wygnanski et al. 1992).

Four correlations suggested by Zhou and Wygnanski (1993) are employed in the present study to predict the behavior of the wall jet in the presence of the external stream and tangential suction. These correlations are as follows:

$$\left.\begin{aligned} F_1(\xi) &= \frac{y_0 J}{R\nu^2}, \\ F_2(\xi) &= \frac{y_m J}{\nu^2}, \\ F_3(\xi) &= \frac{\tau_w R}{\rho}\left(\frac{\nu}{J}\right)^2, \\ F_4(\xi) &= \frac{U_m \nu R}{J} \end{aligned}\right\} \tag{3.14}$$

Zhou and Wygnanski (1993) further suggested the following power laws to express the correlations in Eq. (3.14), where A_1, A_2, A_3, A_4, n_1, n_2, n_3 and n_4 are empirically determined constants:

$$\left.\begin{aligned} F_1(\xi) &= A_1(\xi)^{n_1}, \\ F_2(\xi) &= A_2(\xi)^{n_2}, \\ F_3(\xi) &= A_3(\xi)^{n_3}, \\ F_4(\xi) &= A_4(\xi)^{n_4} \end{aligned}\right\} \tag{3.15}$$

The plots of these functions are presented in Figure 3.39 to Figure 3.42.

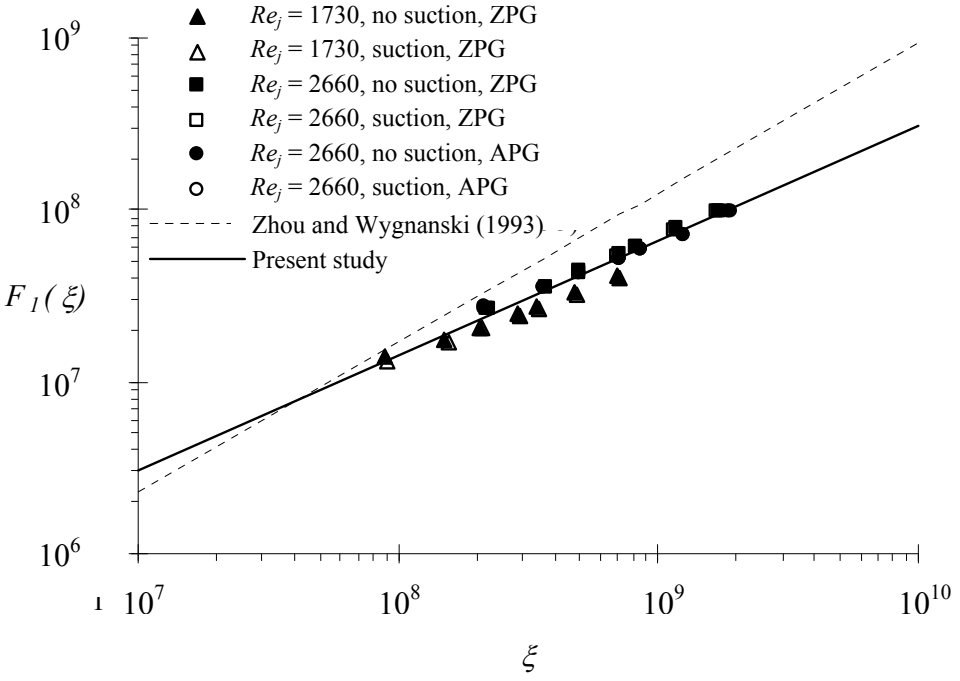

Figure 3.39. Correlation function $F_1(\xi)$.

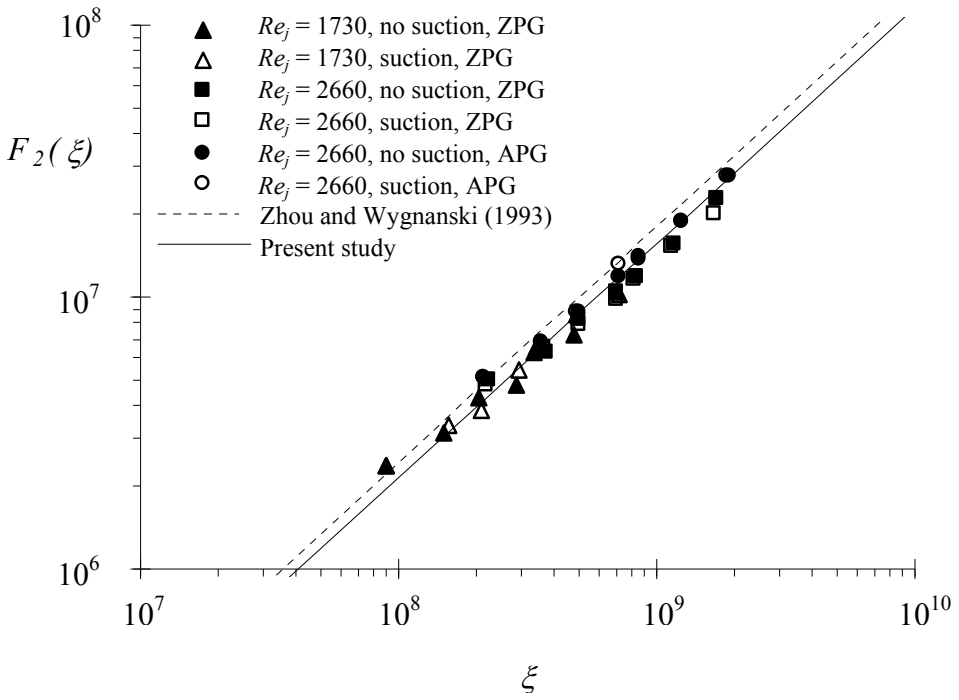

Figure 3.40. Correlation function $F_2(\xi)$.

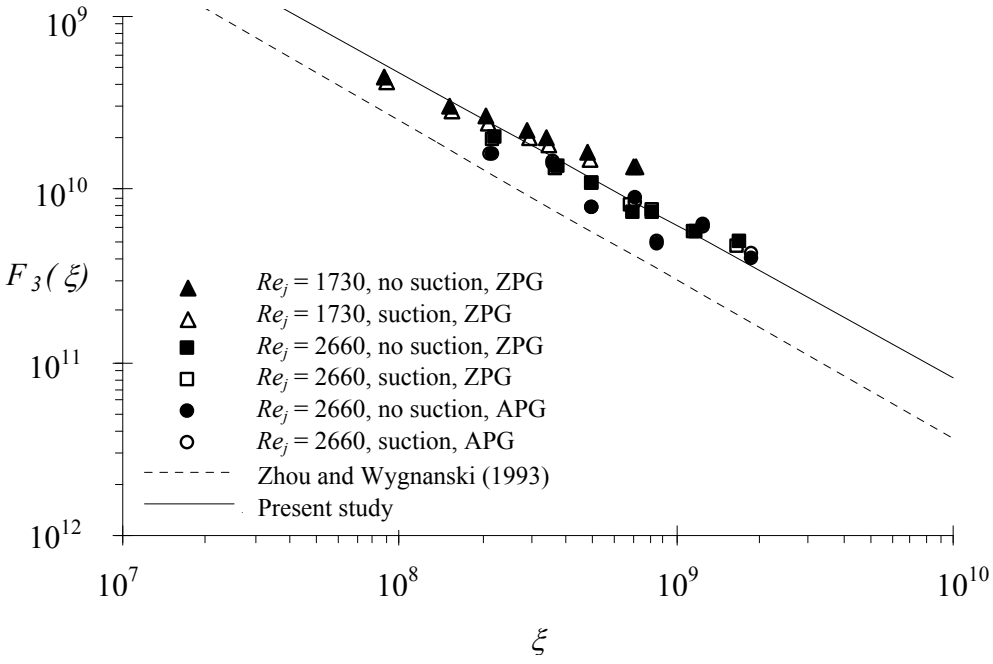

Figure 3.41. Correlation function $F_3(\xi)$.

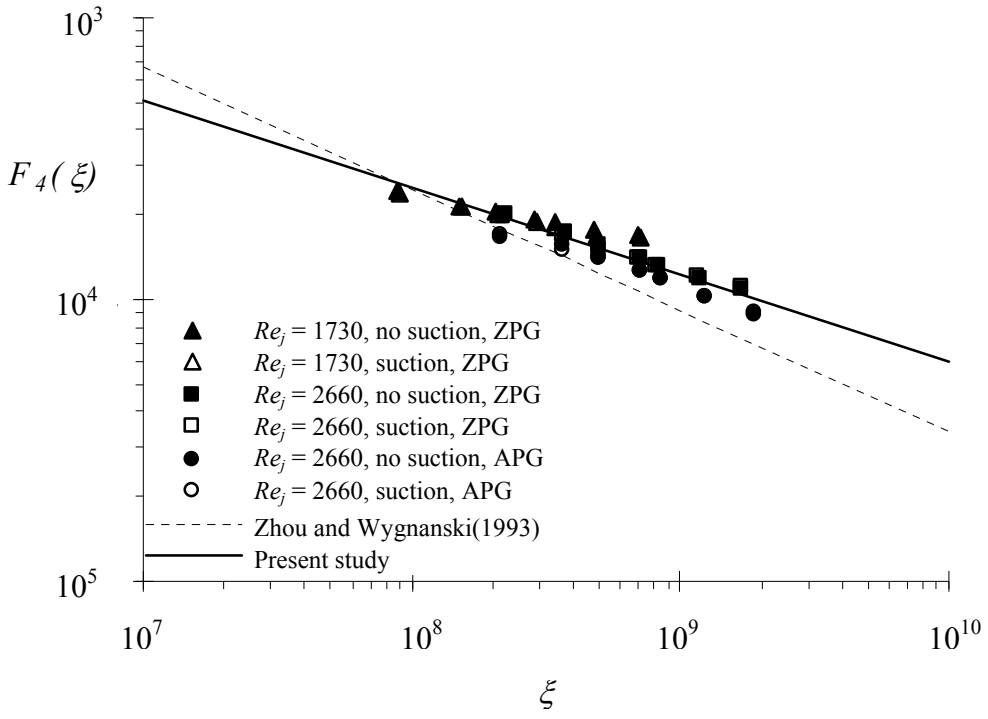

Figure 3.42. Correlation function $F_4(\xi)$.

All the cases considered in the present study are included except where the ratio of $U_\infty/U_m \leq 0.8$. Also included are linear regression lines (solid lines) applied to the log plots as well as the power functions proposed by Zhou and Wygnanski (1993) in their study (dashed lines) for comparison.

All the data from the various cases appear to collapse onto a single regression line for each function except for $F_1(\xi)$. As observed many times previously, no clear distinction is observed between the cases without suction and the corresponding cases with suction. The adverse pressure gradient does not affect the curve as both cases for Re_j = 2660 with and without the adverse pressure gradient collapse well with each other. While the solid regression line for $F_1(\xi)$ is fitted to the log plot to accommodate all the data at both jet Reynolds numbers, the data points for Re_j = 1730 consistently

lie below this line, while those for Re_j = 2660 with and without the adverse pressure gradient lie consistently slightly above this line. Since $F_1(\xi)$ relates to the growth of the wall jet width, this suggests that the jet with the higher jet Reynolds number has a higher growth rate when compared to the one with the lower jet Reynolds number. Although the jet Reynolds number varies by only about one and half times between 1730 and 2660, the velocity and turbulence data shows a significant improvement in terms of data collapse for the higher jet Reynolds number cases. It appears that the effect of Reynolds number within this range of Re_j is significant. The higher Reynolds number may result in greater mixing and entrainment of the flow, leading to a more rapid jet growth.

Figure 3.39 also suggests that the jets for the present study have a relatively slower growth rate compared to Zhou and Wygnanski's (1993). Noting the previous remarks regarding jet Reynolds number effects, and considering that the jet Reynolds number in Zhou and Wygnanski's (1993) study varies from 7000 to 18000, it is not too surprising that the jet growth for the present study is lower than Zhou and Wygnanski's (1993). This confirms the trend found in the present study of increasing jet growth rates with increasing jet Reynolds number. Although the effect of Reynolds number is not obvious from the velocity and turbulence distributions as their collapse at the higher Re_j of 2660 from the present study collapses just as well as those by Zhou and Wygnanski at their much higher Reynolds number, their effects on the jet development become obvious when the data is plotted in the way shown in Figure 3.39. The results suggest that at higher jet Reynolds numbers, the jet growth rate increases, possibly due to the increased mixing and fluid entrainment that occurs

with a higher jet Reynolds number. The virtual origin is also observed to decrease and approaches the actual location of the jet nozzle as Re_j increases, shown by the decrease in the value of the vertical intercept in Figure 3.39.

Although the value of A obtained in the present study as tabulated in Table 3.2 for $F_1(\xi)$ differs greatly from that obtained by Zhou and Wygnanski (1993), Figure 3.39 shows that the plotted values are actually not very far from the regression line obtained from their data. The very large value arises due to the use of a log scale on the plot.

Table 3.2 List of constant of power function expressed in Eq. (3.12)

F(ξ)	Zhou and Wygnanski (1993)		Present Study	
	A_i	n_i	A_i	n_i
$F_1(\xi) = A_1(\xi)^{n_1}$	1.857	0.870	62.81	0.668
$F_2(\xi) = A_2(\xi)^{n_2}$	0.270	0.870	0.270	0.863
$F_3(\xi) = A_3(\xi)^{n_3}$	0.0057	-0.920	0.0057	-0.885
$F_4(\xi) = A_4(\xi)^{n_4}$	0.680	-0.430	0.073	-0.309

The curve for $F_2(\xi)$ compares very favorably with that of Zhou and Wygnanski (1993). Table 3.2 shows the similarity of the obtained coefficients. The collapse of the various cases for this function is also very good. One reason might be due to the relative ease in locating y_m for the relatively thin wall jets and thus enable the accurate calculation of $F_2(\xi)$. The close similarity for the values of $F_2(\xi)$ obtained in these two studies with different Reynolds numbers also suggest that the Reynolds number does not affect the growth of y_m significantly.

$F_3(\xi)$ on the other hand compares more poorly with Zhou and Wygnanski's (1993) proposed functions, and with relatively greater scatter observed in the present data.

The scatter is most likely due to the difficulty in determining the values of the wall shear stress accurately. These values are calculated from the linear slope of the measured velocity profiles near the wall at $3 < y^+ < 7$. A typical example of these near wall profiles is shown in Figure 3.18 where the linear region is clearly observed. The resolution of the vertical probe movement is adjusted such that at least six data points are located in this region. Usually between six to ten data points within the linear region and unaffected by the wall heat transfer (Chew et. al. 1998) are used to determine the near wall velocity gradient as accurately as possible for calculation of the wall shear stress.

The values of $F_3(\xi)$ obtained by Zhou and Wygnanski (1993) lie below that of the present study. Careful observation also shows that the values of $F_3(\xi)$ for Re_j = 2660 lie slightly below that for Re_j = 1730. While this difference is very small and may even be attributed to experimental error, the consistent trend of a decreasing $F_3(\xi)$ with increasing Re_j when taking Zhou and Wygnanski's (1993) results into consideration suggests the possibility that this relationship does exist. $F_3(\xi)$ may be analogous to the skin friction coefficient C_f, which for a boundary layer flow over a flat plate, decreases as the Reynolds number increases (Fernholz and Finley 1996). Although the value of $F_3(\xi)$ may be affected by the Reynolds number, and decreases with increasing Reynolds number, the similar values of A_3 for both the present study and Zhou and Wygnanski's (1993) in Table 3.2 suggests that its rate of decay and therefore also that of the skin friction is similar and relatively unaffected by the jet Reynolds number.

$F_4(\xi)$ (Figure 3.42) in also differs from Zhou and Wygnanski's (1993) proposed functions significantly. A more gradual decay in the jet maximum velocity is observed in the current study, no doubt related to the more gradual jet growth also observed in the present study signified by the gentler gradient of $F_1(\xi)$. A slower jet growth due to reduced mixing and entrainment would understandably lead to a more gradual decay of the jet maximum velocity due to conservation of fluid momentum. The jet Reynolds number effect that resulted in the differences in the $F_1(\xi)$ plot can also be observed in the $F_4(\xi)$, though to a less obvious extent. Careful observation shows that the data shifts downwards as the jet Reynolds number increases, showing that increasing jet Reynolds number increases the rate of decay of the maximum jet velocity.

Zhou and Wygnanski (1993) studied wall jets with Re_j between 7000 and 18000 and were able to conclude from their data that the power laws from these parametric relationships are practically independent of the jet Reynolds number. However, extending these relationships to the present study shows this to be otherwise when the jet Reynolds number is lowered to about 2000. Although Zhou and Wygnanski's (1993) data was for over a larger range of Re_j than that of the present study, the relatively better collapse of all their data compared to the distinction of the present data with Re_j may suggest that the variation with Reynolds number decreases with increasing Reynolds number. This means that the functions may be asymptotic in the limit of infinite Reynolds number.

The effect of the downstream suction is demonstrated to be very limited with regard to the flow development, and the flow is largely dominated by the blowing slot

that essentially issues a plane wall jet. This makes comparisons with other wall jet studies applicable to understanding the development of the present flow. Comparison with the results of Zhou and Wygnanski (1993) have shown the significant effects of the jet Reynolds number on various parameters of the flow development, at least for the range of the Reynolds numbers considered.

Chapter 4: Conclusions

A similarity study of the wall jet flow in the presence of an external stream and tangential suction at zero and adverse pressure gradients have been conducted at jet Reynolds numbers Re_j of 1730 and 2660. Complete self-similarity of such flows has not been found. Instead, self-similar plots have been obtained by using different scaling laws implemented in the outer and inner regions. Using (y_0 - y_m) and (U_0 - U_∞) to scale the vertical coordinate and velocity respectively for the outer regions of the wall jet flow with and without suction results in the satisfactory collapse of much of the mean velocity profiles at both jet Reynolds numbers provided that $U_\infty/U_m \leq 0.8$.

The range of $U_\infty/U_m \leq 0.8$ where the flow exhibits self-similarity of the mean velocity profiles in the present study is wider than the range $U_\infty/U_m \leq 0.5$ suggested by Zhou and Wygnanski (1993). However, it was noted that the self similarity of the mean velocity does not automatically fail when the threshold of $U_\infty/U_m \leq 0.5$ is exceeded. Instead the collapse of the data becomes increasingly poorer as the ratio U_∞/U_m increases. It is likely that the criteria found in the present study which encompasses that of Zhou and Wygnanski's (1993) is a less stringent set by comparison. The limiting U_∞/U_m value depends on how stringent the requirements of self-similarity of the flow are.

Using the outer scale parameters for the inner region results in very poor collapse if at all, while using y_m and U_m to scale the inner region results in relatively better collapse. Even so, the level of data collapse so obtained remains relatively poorer compared to the outer region particularly when the jet Reynolds number is low. The

different scaling used for these two regions suggests the existence of at least two separate regions within the wall jet with flow structures being governed by different parameters in their respective regions.

The difficulty for the inner region data to collapse is consistently observed in both the mean velocity profiles as well as the turbulence intensity profiles near the wall, whether suction is applied or not. Scaling the mean velocity profile using the friction velocity U_τ may improve the collapse of the data very near the wall but does not make the plots independent of Re_j and is therefore not universal. Considering that a free plane jet achieves self-similarity within a relatively much shorter distance, the reason for this consistent lack of similarity in the inner region of a plane wall jet is likely due to viscous friction at the wall hampering the development of equilibrium conditions. Increasing the Reynolds number reduces the effect of this viscosity on the velocity and turbulence profiles and results in a significant improvement in the collapse of the data.

From these scaling attempts, it is concluded that there appears no universal scaling that exists for both the inner and outer regions of the wall jet. Application of similarity laws may require the division of the wall jet into the inner and outer regions with a different scaling required for each region.

By analyzing the boundary layer equations, it is found that if the wall shear stress is ignored, a suitable adverse pressure gradient is required for self-similarity to be achieved for the plane wall jet. Although the present study does not aim to achieve self-similarity by tailoring the required adverse pressure gradient, the imposed adverse pressure gradient obtained by inclining the flat test plate is sufficient to

increase the self-similarity of the flow significantly. The imposed adverse pressure gradient resulted in meeting several conditions determined by Irwin (1973) to be required for self-similarity of the flow, and this is supported by the significant improvement of the collapse in the mean velocity and turbulence data. The analysis only fails near the wall where the assumption of negligible shear stress becomes invalid. In this region near the wall, self-similarity in the mean velocity and turbulence profiles are again not observed.

The application of suction has little significance over the development of the wall jet exiting from the upstream nozzle except very near the suction slot far downstream. Only in the turbulence profiles for the zero pressure gradient cases were the effects of suction observed far upstream where the flow exhibited self-similar behavior. The turbulence intensities for these cases with suction were slightly but consistently lower than their respective cases without suction at all the measurement locations over the test plate. With an adverse pressure gradient imposed however, this upstream effect of suction was no longer observed.

In contrast with a previous work by Zhou and Wygnanski (1993), parameter scaling of the flow relating the three most important parameters of the wall jet y_0, U_m and τ_w to three dimensionless parameters is not completely independent on Reynolds number. While their relationship may appear independent of Reynolds numbers in the range ($Re_j \approx$ 7000-18000) studied by Zhou and Wygnanski (1993), the effect of Reynolds number becomes apparent when that range is increased to include those in the present study at 1730 and 2660. Consistent trends in the relationships are observed with changes in the Reynolds number, with some being affected more than

others. Significantly, increasing the jet Reynolds number increases the jet growth rate and the decay of the jet maximum velocity as predicted by the power laws relations. This is likely due to the increased mixing and fluid entrainment occurring at the higher Reynolds numbers. The effect of the imposed adverse pressure gradient on these relationships is also negligible, appearing to not affect any of the relations.

Bibliography

Avi, S., Greenblatt, D. and Wygnanski, I. Active separation control: an overview of Reynolds and Mach numbers effects, Aerospace Science and Technology Vol. 8, pp. 569-582. 2004

Bruns, J., Dengal, P. and Fernholz, H.H. Mean flow and turbulence measurements in an incompressible two-dimensional turbulent boundary layer. Part I: data. Institutsbericht Nr. 02/92, Herman-Föttinger-Institut für Thermo- und Fluiddynamik, Technische Univerität Berlin. 1992

Barenblatt, G.I., Chorin, A.J., and Prostokishin, V.M. The turbulent wall jet: A triple-layered structure and incomplete similarity, Proceedings of the National Academy of Sciences of the United States of America Vol. 102, No. 25, pp. 8850-8853. 2005

Bradshaw, P. An introduction to turbulence and its measurement, pp. 59-60, Pergamon Press, Oxford. 1975

Bradshaw, P. (ed). Topics in Applied Physics, vol. 12. pp. 60-62, Springer-Verlag, New York. 1976

Chew, Y.T., Khoo, B.C. and Li, G.L. An investigation of wall effects on hot-wire measurements using a bent sublayer probe, Measurement Science and Technology Vol. 9, pp. 67-85. 1998

Englar, R.J. Development of Pneumatic Aerodynamics Devices to Improve the Performance, Economics, and Safety of Heavy Vehicles, SAE 2000-01-2208, 2000

Fernholz, H.H. and Finley, P.J. The incompressible zero-pressure gradient turbulent boundary layer: An assessment of the data, Prog. Aerospace Sci. 32, 4, pp. 245-311. 1996

Gad-el-Hak, M. and Bushnell, D.M. Separation Control: Review, Journal of Fluids Engineering Vol. 113, pp. 5-29. 1991

George, W.K., Abrahamsson, H., Eriksson, J., Karlsson, R., I., Lofdahl, L. and Wosniky, M. A similarity theory for the turbulent plane wall jet without external stream, Journal of Fluid Mechanics Vol. 425, pp. 367-411. 2000

Heap, H. and Crowther, W.J. A review of current leading edge device technology and options for innovation based on flow control, RAeS conference, London, 2003

Irwin, P.A.H. Measurements in a self-preserving plane wall jet in a positive pressure gradient, Journal of Fluid Mechanics Vol. 61, No. 1, pp. 33-63. 1973

Kruka, V. and Eskinazi, S. The wall jet in a moving stream, Journal of Fluid Mechanics Vol. 26, No. 4, pp. 555-579. 1964

Launder, B.E. and Rodi, W. The turbulent wall jet, Progress in Aerospace Sciences Vol. 19, pp. 81–128. 1981

Marineau, E., Schetz, J., and Neel, R. Turbulent navier-stokes simulations of heat transfer with complex wall temperature variations, AIAA No. 2006-3087. 2006

Narasimha, R., Narayan, K.Y. and Parthasarathy, S.P. Parametric analysis of turbulent wall jet in still air, Aeronautical Journal Vol. 77, pp. 335-359. 1973

Neuendorf, R. and Wygnanski, I. On a turbulent jet flowing over a circular cylinder, Journal of Fluid Mechanics Vol. 381, pp. 1-25. 1999

Newman, B.G. Turbulent jets and wakes in a pressure gradient, Sovran, G. (ed) Fluid Mechanics of internal flow, pp. 170-209, Elsevier. 1967

Park, J. and Choi, H. Effects of uniform blowing or suction from a spanwise slot on a turbulent boundary layer flow, Physics of Fluids Vol. 11, pp. 3095-3105. 1999

Patel, R.P. Self-preserving two-dimensional turbulent jets and wall jets in a moving stream, MS Thesis, McGill University. 1962

Patel, V.C. Calibration of the Preston tube and limitations on its use in pressure gradients, Journal of Fluid Mechanics, Vol. 23, pp. 185-205. 1965

Townsend, A.A. The Structure of Turbulent Shear Flow, 2nd ed. pp. 259-263, Cambridge University Press, Cambridge. 1976

Wang, C. and Sun, M. Separation control on a thick airfoil with multiple slots blowing at small speeds, Acta Mechanica Vol. 143, pp. 3-4. 2000

Wygnanski, I., Katz, Y. and Horev, E. On the applicability of various scaling laws to the turbulent wall jet, Journal of Fluid Mechanics, Vol. 234, pp. 669-690. 1992

Zha, G.C. and Gao, W. Analysis of Jet Effects on Co-Flow Jet Airfoil Performance with Integrated Propulsion System, AIAA Paper 2006-0102, AIAA the 44th Aerospace Sciences Meeting and Exhibit Conference, Jan. 8-12, Reno, NV. 2006

Zha, G.C., Gao, W., Paxton, C.D. Numerical Simulation of Co-Flow Jet Airfoil Flows, AIAA Paper 2006-1060, AIAA the 44th Aerospace Sciences Meeting and Exhibit Conference, Jan. 8-12, Reno, NV. 2006a

Zha, G.C., Gao, W., Paxton, C.D. and Palewicz, A. Numerical Investigations of Co-Flow Jet Airfoil with and without Suction, AIAA Paper 2006-1061, AIAA the 44th Aerospace Sciences Meeting and Exhibit Conference, Jan. 8-12, Reno, NV. 2006b

Zha, G.C. and Paxton, C. A Novel Flow Control Method for Airfoil Performance Enhancement Using Co-Flow Jet, Applications of Circulation Control Technologies, edited by Joslin, R.D. and Jones, G.S. AIAA Book Series, Progress in Aeronautics and Astronautics, Vol. 214, Chapter 10, pp. 293-314. 2006

Zhou, M.D. and Wygnanski, I. Parameters governing the turbulent wall jet in an external stream, AIAA Journal Vol. 31, No.5, pp. 848-853. 1993